Induction of Cell Death by Ternary Copper(II) Complexes of L-Tyrosine and Diimines: Role of Coligands on DNA Binding and Cleavage and Anticancer Activity

7 AUTHORS, INCLUDING:

Ramakrishnan Sethu
University of Illinois, Urbana-Champaign
14 PUBLICATIONS **413** CITATIONS

SEE PROFILE

Vaiyapuri Subbarayan Periasamy
King Saud University
52 PUBLICATIONS **707** CITATIONS

SEE PROFILE

Hanumanthappa Krishnamurthy
Tata Institute of Fundamental Research
47 PUBLICATIONS **1,526** CITATIONS

SEE PROFILE

M A Akbarsha
King Saud University
208 PUBLICATIONS **2,079** CITATIONS

SEE PROFILE

Ternary Dinuclear Copper(II) Complexes of a Hydroxybenzamide Ligand with Diimine Coligands: the 5,6-dmp Ligand Enhances DNA Binding and Cleavage and Induces Apoptosis

Sethu Ramakrishnan,[†] Dhanasekaran Shakthipriya,[†] Eringathodi Suresh,[‡] Vaiyapuri Subbarayan Periasamy,[§] Mohammad Abdulkader Akbarsha,[§] and Mallayan Palaniandavar*,[†]

[†]Centre for Bioinorganic Chemistry, School of Chemistry, and [§]Department of Animal Science, Bharathidasan University, Tiruchirapalli 620 024, India

[‡]Analytical Science Discipline, Central Salt and Marine Chemical Research Institute, Bhavnagar 364 002, India

Ⓢ Supporting Information

ABSTRACT: The dinuclear copper(II) complexes $[Cu_2(LH)_2(diimine)_2(ClO_4)_2](ClO_4)_2$ (**1**−**4**), where LH = 2-hydroxy-N-[2-(methylamino)ethyl]benzamide and diimine = 2,2′-bipyridine (bpy; **1**), 1,10-phenanthroline (phen; **2**), 5,6-dimethyl-1,10-phenanthroline (5,6-dmp; **3**), and dipyrido[3,2-d:2′,3′-f]quinoxaline (dpq; **4**), have been isolated and characterized. The X-ray crystal structure of complex **1** contains two copper-(II) centers bridged by the phenolate moiety of the amide ligand. All of the complexes display a ligand-field band (630−655 nm) and the PhO^--to-Cu^{II} ligand-to-metal charge-transfer band (405−420 nm) in solution. Absorption and emission spectral studies and viscosity measurements indicate that complex **4** interacts with calf thymus DNA more strongly than all of the other complexes through strong partial intercalation of the extended planar ring (dpq) with a DNA base stack. Interestingly, **3** exhibits a DNA binding affinity higher than **2**, suggesting the involvement in hydrophobic interaction of coordinated 5,6-dmp with the DNA surface. In contrast to the increase in relative viscosities of DNA bound to **2**−**4**, a decrease in viscosity of DNA bound to **1** is observed, indicating a shortening of the DNA chain length through formation of kinks or bends. All of the complexes exhibit an ability to cleave DNA (pUC19 DNA) in a 5% DMF/5 mM Tris-HCl/50 mM NaCl buffer at pH 7.1 in the absence of an oxidant at 100 μM complex concentration, which varies as **4** > **2** > **1** > **3**. The order of DNA the cleavage ability at 30 μM concentration in the presence ascorbic acid is **4** > **2** > **1** > **3**, and, interestingly, **4** alone shows an ability to convert supercoiled DNA into nicked-coiled DNA even at 6 μM concentration, beyond which complete degradation is observed and the pathway of oxidative DNA cleavage involves hydroxyl radicals. In the presence of distamycin, all of the complexes, except **3**, show decreased DNA cleavage activity, suggesting that the complexes prefer to bind in the DNA minor groove. All of the complexes exhibit prominent DNA cleavage even at very low concentrations (nM) in the presence of H_2O_2 as an activator, with the order of cleavage efficiency being **3** > **2** > **4** > **1**. Studies on the anticancer activity toward HEp-2 human larynx cell lines reveal that the ability of the complexes to kill the cancer cell lines varies as **3** > **4** > **2** > **1**. Also, interestingly, the IC_{50} value of **3** is lower than that of cisplatin, suggesting that the hydrophobicity of methyl groups on the 5 and 6 positions of the complex enhances the anticancer activity. The mode of cell death effected by the complex has been explored by using various biochemical techniques like comet assay, mitochondrial membrane potency, and Western blotting. The complex has been found to induce nuclear condensation and fragmentation in cell lines. Also, it triggers activation of caspases by releasing cytochrome c from mitochondria to cytosol, suggesting that it induces apoptosis in cells via the mitochondrial pathway.
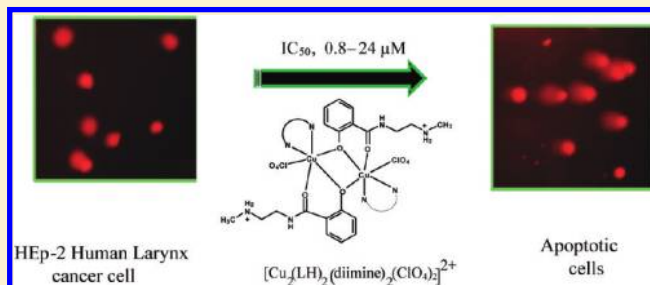
■ INTRODUCTION

Since the discovery of the antitumor activity of cisplatin,[1] numerous mononuclear platinum(II) complexes have been synthesized and their anticancer activities carefully evaluated on appropriate biological models.[2] Several polynuclear platinum complexes of multidentate ligands have been isolated now and are found to form adducts with DNA, which are substantially different from those of cisplatin.[3] Certain classes of platinum(II) complexes with two or three platinum—amine units linked by a diamine chain of variable length have already been shown to be successful in treating cases lacking cross resistance.[4−6] A few dinuclear platinum complexes have been found to act as anticancer drugs better than cisplatin, particularly for treating metastasis. Very recently, the antitumor activity of several cationic trinuclear platinum complexes have been investigated by Farrell et al., and one (BBR-3464) of the complexes has undergone both phase I[7] and phase II[8,9] clinical trials. The trinuclear complex has

been shown to be cytotoxic at concentrations that are 20-fold lower than that of cisplatin, and the increased potency is attributed to its unique DNA binding profile in comparison to mononuclear complexes.[10] All of these polynuclear complexes are involved in novel types of both intra- and interstrand cross-links[11] with DNA, which indeed may have different biological effects. Unfortunately, in contrast to general expectations, most of the platinum(II) complexes investigated so far exhibit biological activities very similar to those of cisplatin with almost superimposable properties and, thus, with no significant therapeutic advantage. Also, the types of cancer that can be treated with platinum drugs are very few, and the drugs suffer from side effects and resistance phenomena.[12,13] So, many other novel transition-metal complexes as well as small-molecule-based antitumor agents have been developed, and some of them are under clinical trial.[14a−e]

Copper(II) complexes are considered the best alternatives to cisplatin because copper is biocompatible and exhibits many significant roles in biological systems. Also, synthetic copper(II) complexes have been reported to act as pharmacological agents and as potential anticancer and cancer-inhibiting agents.[15−20] Also, very recently, certain mixed-ligand copper(II) complexes, which strongly bind and cleave DNA, exhibit prominent anticancer activities and regulate apoptosis.[21−25] Very recent studies have demonstrated that certain multinuclear copper(II) complexes can efficiently promote DNA cleavage by selectively oxidizing deoxyribose or nucleobase moieties.[26] The copper centers in some multinuclear complexes act synergistically to cleave DNA with higher efficiency or selectivity.[26−30] Karlin and co-workers[31,32] have shown that nuclearity is a crucial parameter in oxidative DNA cleavage, with the synergy between the metal ions contributing to the high nucleolytic efficiency of polynuclear copper(II) compounds. Therefore, designing suitable multinuclear copper complexes for DNA binding and cleavage under both oxidative and hydrolytic conditions, depending upon the recognition elements in the ligand, is of remarkable importance in considering the advantages of processes that produce fragments similar to those formed by restriction enzymes.[26,27] So, in the present investigation, we have isolated redox-active mixed-ligand dinuclear copper(II) complexes of the general formula $[Cu_2(LH)_2(diimine)_2(ClO_4)_2](ClO_4)_2$ (**1**−**4**), where LH is 2-hydroxy-*N*-[2-(methylamino)ethyl]benzamide and diimine is 2,2′-bipyridine (bpy; **1**), 1,10-phenanthroline (phen; **2**), 5,6-dimethyl-1,10-phenanthroline (5,6-dmp; **3**), or dipyrido[3,2-*d*:2′,3′-*f*]quinoxaline (dpq; **4**) (Scheme 1), and investigated their DNA binding and cleavage properties and anticancer activities. The bidentate diimine coligand is expected to function as a DNA recognition element, while the tridentate benzamide functions as the primary ligand. There has been considerable attention focused on the use of small metal complexes containing diimines as metal-based synthetic nucleases.[26−29] Very recently, we have found that the diimine coligands in mixed-ligand copper(II)[24,25] and ruthenium(II)[33] complexes play a pivotal role in the mechanism underlying induction of cell death.

It is proposed to employ electronic absorption and emission spectral and viscosity studies to diagnose the mode and extent of interaction of the dinuclear copper(II) complexes with DNA and then to understand the DNA cleavage abilities and anticancer activities of the complexes in terms of their DNA binding affinity. Also, we have chosen to study the in vitro cytotoxicity of the DNA-cleaving dinuclear copper(II) complexes toward HEp-2 human larynx cancer cell lines. It is remarkable that the 5,6-dmp

Scheme 1. Dinuclear Copper(II) Complexes 1−4 of Diimine Ligands
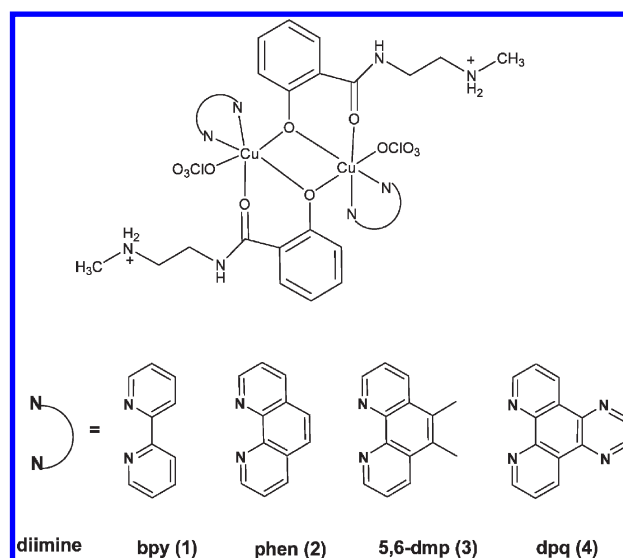
complex, which binds to DNA through hydrophobic forces of interaction, exhibits a strong potential to act as a novel antitumor agent in micromolar concentrations.

■ RESULTS AND DISCUSSION

Syntheses and Structures of Complexes. Mixed-ligand dinuclear copper(II) complexes of the type $[Cu_2(LH)_2(diimine)_2(ClO_4)_2](ClO_4)_2$ (**1**−**4**), where LH = 2-hydroxy-*N*-[2-(methylamino)ethyl]benzamide and diimine = 2,2′-bipyridine (bpy; **1**), 1,10-phenanthroline (phen; **2**), 5,6-dimethyl-1,10-phenanthroline (5,6-dmp; **3**), and dipyridoquinoxaline (dpq; **4**),[35] have been isolated by adding a methanolic solution of hydrated copper(II) perchlorate to a mixture of the ligand LH and diimine in a methanol solution. All of the complexes have been obtained in good yields and characterized by elemental analysis, electrospray ionization mass spectrometry (ESI-MS), and UV−visible spectral technique. The X-ray crystal structure of **1** reveals that it contains a dimeric copper unit, and related complexes **2**−**4** are suggested to contain the same structure, which is supported by ESI-MS data. Complexes **1** and **2** are soluble in a 5 mM Tris-HCl/50 mM NaCl buffer at pH 7.1, while **3** and **4** are soluble in a 5% DMF/5 mM Tris-HCl/50 mM NaCl buffer at pH 7.1. For the present study, solutions of the complexes were prepared in a 5% DMF/5 mM Tris-HCl/50 mM NaCl buffer at pH 7.1. In a 5% DMF/5 mM Tris-HCl/50 mM NaCl buffer at pH 7.1, all of the complexes exhibit only one broad band in the visible region (630−655 nm) with very low absorptivity (Table S1 in the Supporting Information), which is consistent with the square-based geometry of copper(II) observed in the solid-state structure of **1**. The intense absorption bands observed in the regions of 239−282 and 405−420 nm are attributed to the intraligand $\pi \rightarrow \pi^*$ transitions within the coordinated phenolate moiety and diimines and the PhO$^-$ → copper(II) ligand-to-metal charge-transfer (LMCT) transitions, respectively. ESI-MS spectral data (Figure S1 in the Supporting Information) suggest that the perchlorate anions are strongly bound to copper in the dimeric complex. This is supported by conductivity measurements in aqueous solution and in an
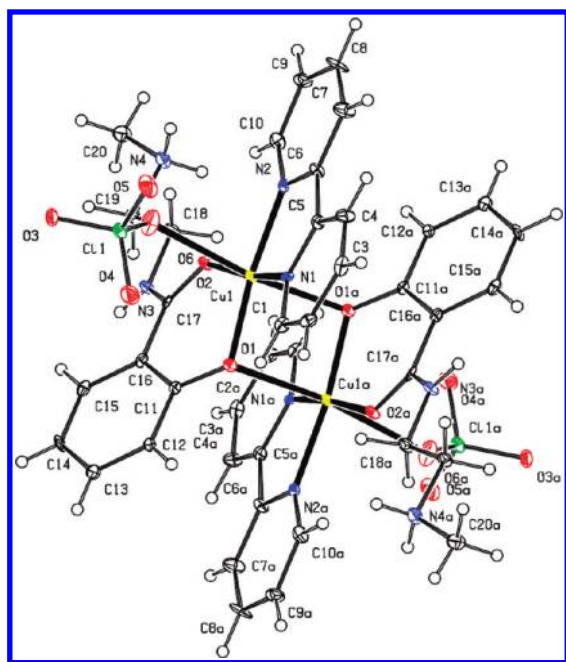
Figure 1. ORTEP representation of complex cation **1** showing the atom numbering scheme and displacement ellipsoids (50% probability level).

Table 1. Crystal Data and Structure Refinement Details for Complex 1

	1
empirical formula	$Cu_2C_{40}H_{44} Cl_4N_8O_{20}$
fw	1225.73
cryst syst	triclinic
space group	$P\bar{1}$
a, Å	9.6719(12)
b, Å	11.4218(14)
c, Å	11.9689(15)
α, deg	109. 261(2)
β, deg	106. 116(2)
γ, deg	94. 474(2)
V, Å	1178.0(3)
Z	1
λ, Å	Mo Kα, 0.710 73
D_{calc}, g cm^{-3}	1.728
GOF on F^2	1.093
θ for data collection	1.9−25.0
final R indices $[I > 2\sigma(I)]$	0.0656
R1^a	0.1317
wR2^a	

^{a} R1 = $\Sigma||F_o| - |F_c||/\Sigma|F_o|$; wR2 = $\{\Sigma w[(F_o^2 - F_c^2)^2/\Sigma w[(F_o^2)^2]\}^{1/2}$.

Table 2. Selected Interatomic Distances and Angles for Complex 1

bond distances (Å)		bond angles (deg)	
Cu1−N1	1.979(5)	O1−Cu1−N1	93.75(17)
Cu1−N2	1.993(4)	O1−Cu1−N2	172.74(17)
Cu1−O1	1.902(3)	O1−Cu1−O1_a	84.47(14)
Cu1−O1_a	2.421(4)	O1−Cu1−O2	91.83(15)
Cu1−O2	1.938(4)	O1−Cu1−O6	103.22(15)
Cu1−O6	2.582(4)	O2−Cu1−O6	84.80(15)
		O2−Cu1−N1	170.19(17)
		O2−Cu1−N2	93.63(16)
		O1_a−Cu1−O2	91.82(15)
		O6−Cu1−N1	86.08(16)
		O6−Cu1−N2	82.06(16)
		O1_a−Cu1−O6	171.66(13)
		N1−Cu1−N2	81.55(18)
		O1_a−Cu1−N1	96.74(16)
		O1_a−Cu1−N2	90.57(15)

aqueous *N,N*-dimethylformamide (DMF; 2%) solution (Λ_M, 210−325 Ω^{-1} cm^2 mol^{-1}; Table S2 in the Supporting Information), which fall in the range[34] for 1:2 electrolytes. The electron paramagnetic resonance spectra of the complexes are silent, suggesting that their two copper(II) centers are strongly antiferromagnetically coupled.

Description of the Crystal Structure of [Cu₂(LH)₂-(bpy)₂(ClO₄)₂](ClO₄)₂ (1). An ORTEP view of the complex cation $[Cu_2(LH)_2(bpy)_2(ClO_4)_2]^{2+}$ with the atom numbering scheme is shown in Figure 1. Selected bond lengths and angles for **1** are listed respectively in Tables 1 and 2. The distorted octahedral environment around each copper(II) in the dimeric complex is constituted of the two nitrogen atoms (N1 and N2) of 2,2′-bipyridine, the carbonyl (O1) and phenolate (O2) oxygen atoms of the N-protonated bidentate amide ligand, the oxygen atom (O6) of the perchlorate anion, and the coordinated phenolate oxygen atom (O1_a) of the second amide ligand coordinated to the other copper(II). The Cu−N$_{bpy}$ distances observed [Cu1−N1, 1.978(5) Å; Cu1−N2, 1.992(4) Å] fall within the range for Cu−N$_{imine}$ distances observed for other diimine complexes already reported.[32] The amide O1 [Cu1−O1, 1.902(3) Å] and phenolate (O2) oxygen atoms [Cu1−O2, 1.939(4) Å] are bound to copper(II) in the equatorial plane at distances shorter than those of the phenolate [Cu1−O1_a, 2.420(4) Å] and perchlorate oxygen atoms [Cu1−O6, 2.583(4) Å] occupying the axial positions, which is expected from the presence of two electrons in the d$_{z2}$ orbital of copper-(II). The tetragonally distorted ($T = 0.781$)[36] octahedral complex shows static Jahn−Teller distortion as a consequence of crystal packing. The dimerization in the complex is because of the absence of a strong donor atom in the equatorial position[37] of the neutral complex, which leads to the coordinated phenolate group in the neighboring molecule to default to the equatorial position in the first molecule. Interestingly, the two phenolates are coordinated in a cis-axial/equatorial fashion, with the equatorial

Cu−O1 bond [1.902(3) Å] being shorter than the axial Cu−O1_a bond [2.420(4) Å].

DNA Binding Studies: Absorption Spectral Studies. Upon the addition of a solution of calf thymus (CT) DNA to the copper(II) complexes, a decrease in the absorption intensities (hypochromism, $\Delta\varepsilon$, 66−96%; Figure 2) of the $\pi \rightarrow \pi^*$ absorption bands of **2−4** with red shifts (2−8 nm) in the band positions is observed, indicating strong DNA binding of the complexes. In contrast, an increase in the intensity (hyperchromism, $\Delta\varepsilon$, 57%; Figure S2 in the Supporting Information) of the band with no shift in the band position is observed for **1**, suggesting a mode of DNA binding for the complex different

from that of others. Because the extent of hypochromism is commonly associated with the strength of intercalative interaction,[38−40] the observed trend in hypochromism, **4 > 3 > 2**, reflects a decrease in the DNA binding affinities of the complexes in this order (Figure S2 in the Supporting Information). From the observed spectral changes, the value of the intrinsic equilibrium DNA binding constant (K_b) was determined for **2−4** by using the equation[41]

$$[DNA]/(\varepsilon_a - \varepsilon_f) = [DNA]/(\varepsilon_b - \varepsilon_f) + 1/K_b(\varepsilon_b - \varepsilon_f)$$

where [DNA] is the concentration of CT DNA in the base pairs, ε_a is the apparent extinction coefficient obtained by calculating $A_{obs}/[complex]$, ε_f corresponds to the extinction coefficient of the complex in its free form, and ε_b refers to the extinction coefficient of the complex in the bound form. Each set of data, when fitted to the above equation, gives a straight line with a slope of $1/(\varepsilon_b - \varepsilon_f)$ and a y intercept of $1/K_b(\varepsilon_b - \varepsilon_f)$, and the ratio of the slope to intercept gives the value of the intrinsic binding constants (Figure 2). The K_b values of the complexes $[(0.5-7.6) \times 10^4]$ follow the order **4 > 3 > 2** (Table 3), which is consistent with the above order of hypochromism. They are much lower than those observed[42] for the typical classical intercalator ethidium bromide (EthBr; K_b, 4.94×10^5 M^{-1} in a 25 mM Tris-HCl/40 mM NaCl buffer, pH 7.9) and the partially intercalating complex cation[43] $[Ru(bpy)_2(dpq)]^{2+}$ (K_b, 1.4×10^6 M^{-1} in a 25 mM Tris-HCl/40 mM NaCl buffer, pH 7.9), both bound to CT DNA. So, it is obvious that the highest DNA binding affinity as well as the largest red shift (**2**, 6 nm; **3**, 2 nm; **4**, 8 nm) observed for **4** are due to the larger surface area of the aromatic ring of the dpq ligand, which enhances the extent of its stacking with DNA base pairs. The incorporation of the methyl groups on the 5 and 6 positions of the phen ring as in **3** would be
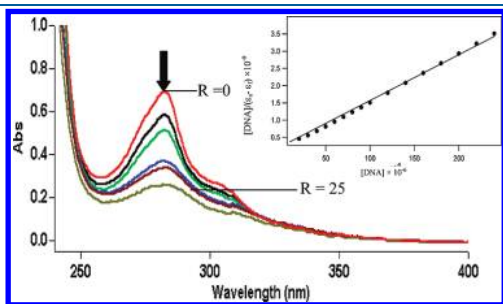
expected to hinder the partial intercalation of the phen ring and, hence, lead to a DNA binding affinity lower than that of the phen complex **2**. However, a higher DNA binding affinity is observed for **3**, suggesting that the complex is involved in DNA groove binding rather than intercalative DNA binding. This is supported by the lower red shift observed for **3** (2 nm). Similar observations were made by us earlier for the simple mononuclear complexes $[Cu(5,6\text{-}dmp)_3]^{2+}$, $[Zn(5,6\text{-}dmp)_3]^{2+,36}$ and $[Ru(5,6\text{-}dmp)_3]^{2+,44}$ the mixed-ligand mononuclear complexes $[Ru(5,6\text{-}dmp)(NH_3)_4]^{2+,45}$ $[Cu(imda)(5,6\text{-}dmp)]^{,46}$ $[Cu(dipica)(5,6\text{-}dmp)]^{2+,47}$ and $[Cu(L\text{-}tyr)(5,6\text{-}dmp)]^+$ (L-tyr = L-tyrosine),[25] and the dinuclear complex $[\{(5,6\text{-}dmp)_2Ru\}_2(bpm)]^{4+48}$ bound to CT DNA. Complex **1** with two noncoplanar pyridine rings is obviously not involved in partial intercalative interaction but in the electrostatic binding to DNA via the exterior of phosphate esters. Thus, the number of aromatic rings in the diimine coligand and the substituent on the phen ring dictate the DNA binding affinity and binding structure of the present mixed-ligand complexes. Also, the diimine coligands rather than the primary ligand play a vital role in determining the mode as well as the extent of DNA binding of the complexes.

EthBr Displacement Assay. Upon the addition of complexes **1−4** (0−60 μM) to CT DNA pretreated with EthBr ([EthBr]/[DNA] = 0.1) in a 5% DMF/5 mM Tris-HCl/50 mM NaCl buffer at pH 7.1, the emission intensity of DNA-bound EthBr decreases. From a plot of the observed intensities against the complex concentration, the values of the apparent DNA binding constant (K_{app}) were calculated using the equation[49]

$$K_{EthBr}[EthBr] = K_{app}[complex]$$

where K_{EthBr} (4.94×10^5 M^{-1})[42] is the DNA binding constant of EthBr, [EthBr] is the concentration of EthBr (12.5 μM), and [complex] is the concentration of the complex used to obtain 50% reduction in the fluorescence intensity of EthBr. The observed decrease in the emission intensity of EthBr (Figure 3) and, hence, the DNA binding affinities of the complexes follow the order **4 > 3 > 2 > 1** (Table 3), which is in conformity with the order of DNA binding affinities obtained from the absorption spectral (cf. above) and viscosity studies (cf. below). Both the electron transfer from excited EthBr to copper(II) and the EthBr displacement mechanisms would account for the highest value of K_{app} determined for the partially intercalating complex **4**. At higher concentrations, the latter would compete efficiently with the intercalatively bound EthBr for DNA binding and quench the EthBr emission more strongly than **1−3**. We propose that hydrogen-bonding interactions, which would occur between the ligand $-N(Me)H_2^+$ moieties in the dinuclear copper(II) complex and DNA, would also

Figure 2. Absorption spectra of **3** (2×10^{-5} M) in a 5% DMF/5 mM Tris-HCl/50 mM NaCl buffer at pH 7.1 in the absence ($R = 0$) and presence of ($R = 25$) of increasing amounts of CT DNA. Inset: Plot of [DNA] vs [DNA]/($\varepsilon_a - \varepsilon_f$) at $R = 25$ of **3**.

Table 3. Ligand-Based Absorption Spectral Properties and Fluorescence Spectral Properties of Copper(II) Complexes Bound[a] to CT DNA

complex	λ_{max} (nm)	R	change in the absorbance	$\Delta\varepsilon$ (%)	red shift (nm)	$K_b \times 10^4$ (M^{-1})	$K_{app} \times 10^5$ (M^{-1})[b]
$[Cu_2(LH)_2(bpy)_2(ClO_4)_2]^{2+}$	239	25	hyperchromism	57	0		0.5
$[Cu_2(LH)_2(phen)_2(ClO_4)_2]^{2+}$	273	25	hypochromism	66	6	0.5 ± 0.1	0.7
$[Cu_2(LH)_2(5,6\text{-}dmp)_2(ClO_4)_2]^{2+}$	282	25	hypochromism	81	2	2.3 ± 0.5	1.3
$[Cu_2(LH)_2(dpq)_2(ClO_4)_2]^{2+}$	257	25	hypochromism	96	8	7.6 ± 0.8	3.4

[a] Measurement made at $R = 25$, where $R = [DNA]/[Cu complex]$ and the concentrations of copper(II) complex solutions are 3.0×10^{-5} M (**1**), 2.0×10^{-5} M (**2**), 1.0×10^{-5} M (**3**), and (**4**). [b] Measurement at $1/R = 25$, where $1/R = [Cu complex]/[DNA]$ and the concentration of the DNA solution is 125 μM.
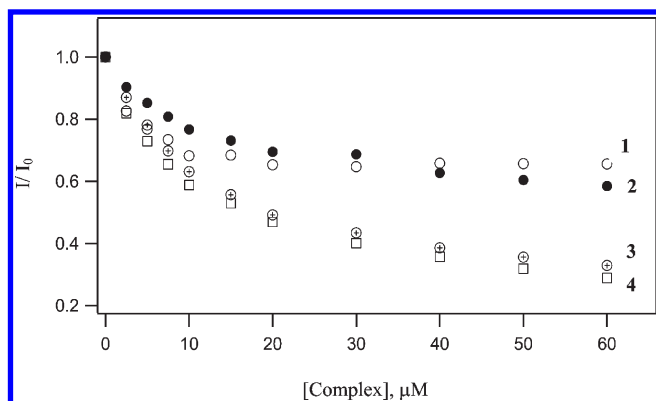
Figure 3. Effect of the addition of complexes **1–4** on the emission intensity of the CT DNA-bound EthBr at different complex concentrations in a 5% DMF/5 mM Tris-HCl/50 mM NaCl buffer at pH 7.1 at 25 °C.
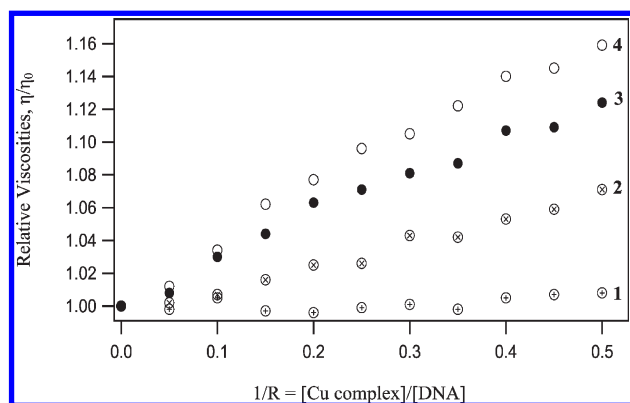

Figure 4. Effect of the addition of complexes **1–4** to CT DNA: relative viscosities vs $1/R$; [CT DNA] = 500 μM.

contribute significantly to the higher DNA binding affinity of **4**. The complex **3** interacts with DNA through hydrophobic methyl groups on the 5 and 6 positions of the phen ring, which is more important than the partial intercalation of the phen ring in **2** in determining the extent of EthBr quenching.

Viscosity Measurements. In order to understand the nature and mode of DNA binding of the dinuclear complexes, viscosity measurements were carried out. The values of the relative specific viscosity (η/η_0), where η and η_0 are the specific viscosities of DNA in the presence and absence of the complexes, are plotted against $1/R$ ($=$[complex]/[DNA] = 0.05–0.5; Figure 4). The ability of the complexes to increase the viscosity of DNA depends upon the diimine ligand: dpq (**4**) > 5,6-dmp (**3**) > phen (**2**) > bpy (**1**). The increase in the viscosity observed for the dpq complex is significantly higher than that for the phen complex, but it is less than that for the potential intercalator EthBr.[50] The partial insertion[51] of the coordinated dpq ligand of **4** in between the DNA base pairs (cf. above) is deeper than that of the coordinated phen ligand of **2**. The DNA groove binding of **3** via the hydrophobic interaction of the coordinated 5,6-dmp ligand is more effective than the partial intercalation of the phen ring in **2** in lengthening the DNA duplex. A similar enhanced viscosity has been observed for simple $(5,6\text{-dmp})_3\text{Fe}^{II}$,[52] -Co^{II},[53] -Ni^{II},[53] -Cu^{II},[36] and -Zn^{II}[36] complexes and mixed-ligand copper-(II) complexes with 5,6-dmp as the coligand.[45–48] In contrast to
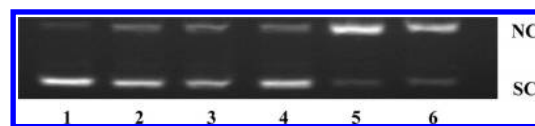

Figure 5. DNA cleavage of (40 μM) complexes **1–4** with an incubation time of 1 h in a 5% DMF/5 mM Tris-HCl/50 mM NaCl buffer at pH 7.1: lane 1, DNA control; lane 2, DNA + **1**; lane 3, DNA + **2**; lane 4, DNA + **3**; lane 5, DNA + **4**; lane 6, DNA + $[\text{Cu(dpq)}_2]^{2+}$. The complex concentration is 100 μM for lanes 2–6. SC and NC are supercoiled and nicked-circular forms of DNA, respectively.

Table 4. Self-Activated Cleavage Data of SC pUC19 DNA (40 μM in Base Pairs) by Complexes 1–4 (0.1 mM) in the Absence of Any Reducing Agent for an Incubation Time of 1 h

serial no.	reaction conditions	form %	
		SC	NC
1	DNA control	92.1	7.9
2	DNA + **1**	71.5	28.5
3	DNA + **2**	63.2	36.8
4	DNA + **3**	74.2	25.8
5	DNA + **4**	11.5	88.6
6	DNA + $[\text{Cu(dpq)}_2(\text{H}_2\text{O})](\text{ClO}_4)_2$	10.0	90.0

2–4, complex **1** shortens the DNA chain length by forming bends or kinks on the DNA double helix upon binding to the DNA surface, which is in conformity with its lowest DNA binding affinity (cf. above). Thus, viscosity studies are in conformity with the hypochromism and K_b and K_{app} values observed for the complexes (cf. above) and confirm that the central rings of dpq (**4**) and phen (**2**) are involved in the partial intercalative mode of DNA binding while the 5,6-dmp (**3**) and bpy (**1**) complexes are involved in DNA groove and electrostatic binding, respectively.

DNA Cleavage Studies: DNA Cleavage without Added Reductant. To explore the DNA cleavage abilities of **1–4**, supercoiled (SC) pUC19 DNA (40 μM in base pairs) was incubated at 37 °C with the complexes in a 5% DMF/5 mM Tris-HCl/50 mM NaCl buffer at pH 7.1 for 1 h in the absence of an activator. All of the complexes cleave SC DNA (form I) into NC DNA (form II) (Figure 5), and the DNA cleavage efficiencies follow the order **4** (88.6) > **2** (36.8) > **1** (28.5) > **3** (25.8%) (Table 4). This reveals that **4** cleaves DNA more efficiently than the other complexes, obviously because of involvement in the strong partial intercalation of the extended aromatic ring of the dpq ligand. Also, the DNA cleavage efficiencies of **1–4** are lower than those of their corresponding bis(diimine)copper-(II) complexes like $[\text{Cu(dpq)}_2]^{2+}$, which exhibits ~100% DNA cleavage.[54] Control experiments with ligand, $\text{Cu(ClO}_4)_2$·$6\text{H}_2\text{O}$, or DNA alone did not reveal any cleavage. Complex **4**, which exhibits the strongest DNA binding affinity and effective DNA cleavage efficiency, was subjected to further cleavage studies. Upon variation of the concentration of **4** with a constant concentration of SC pUC19 DNA (40 μM) under "pseudo-Michaelis–Menton", concentration-dependent DNA cleavage is observed in a 5% DMF/5 mM Tris-HCl/50 mM NaCl buffer at pH 7.1 and 37 °C (Table 5). The kinetic parameters k_{cat} (1.61 $\pm$ 0.13 h^{-1}) and K_M (1.35 μM) at an incubation time of 60 min were calculated based on the plots

obtained (Figure 6A,B). The rate of cleavage of ds-DNA [$(7.7 \pm 0.6) \times 10^6$ h^{-1}] for **4** is enormously higher than the uncatalyzed rate $(3.6 \times 10^{-8}$ h$^{-1})$.[55] The cleavage reaction was performed also by variation of the DNA concentration and keeping the complex concentration constant under a "true Michaelis−Menton" kinetic condition with an incubation period of 60 min. The rate constant observed for **4** is $(6.7 \pm 0.3) \times 10^6$ h^{-1} (Figure S3A,B in the Supporting Information). However, the rate of DNA cleavage is slightly lower than those of $[Cu(dpq)_2]^{2+}$ [54] and mononuclear mixed-ligand copper(II) complexes.[24,25] The extent of DNA cleavage varies exponentially with the incubation time. The plots of disappearance of form I (SC DNA) and the appearance of form II (NC) versus time follow pseudo-first-order kinetic profiles and fit well into a single-exponential curve at constant complex and DNA concentrations (Figure S4 and Table S3 in the Supporting Information).

The preliminary mechanism of DNA strand scission by **4** has been investigated in the presence of several addends under an inert atmosphere. When the hydroxyl radical scavenger dimethyl sulfoxide (DMSO) is added to the reaction mixture, inhibition of DNA cleavage is observed, revealing that the cleavage reaction involves $^{\bullet}$OH radicals. The addition of NaN$_3$ scarcely protects DNA against strand breakage induced by **4**, which suggests that neither $^1O_2$ nor any other singlet oxygen-like entity participates in the oxidative DNA cleavage. This attenuation of the cleavage activity can be explained by taking into consideration the reduction of Cu^{II} ion in the reactive oxygen species (ROS) production process. Also, the addition of catalase enzyme blocks the breakdown of DNA, suggesting that hydrogen peroxide

participates in the cleavage process. However, the addition of the minor groove binder distamycin decreases the ability of the complex to cleave DNA, suggesting that the complex prefers to bind in the DNA minor groove. Further, the addition of super-oxide dismutase (superoxide scavenger) to the reaction mixture does not quench the cleavage reaction significantly, revealing that superoxide anion is also not the active species.[56]

DNA Cleavage with Added Reductant. The DNA strand scission by **1**−**4** was studied in a 5% DMF/5 mM Tris-HCl/50 mM NaCl buffer at pH 7.1 using plasmid SC pUC19 DNA as a substrate in the presence of activators[57−59] (ascorbic acid or H$_2$O$_2$), and the reaction mixture was incubated at 37 °C for 1 h. The cleavage abilities of the complexes in the presence of ascorbic acid under identical conditions were assessed from conversion of DNA from the supercoiled form (SC DNA, form I) to the nicked-circular form (NC DNA, form II). At 30 μM complex concentration, **4** completely degrades SC DNA into undetectable minor fragments (Figure 7 and Table 6) while **1** (NC form, 97%) and **2** (NC form, 98%) cause DNA cleavage more prominent than **3** (NC form, 92%). In the control experiments with DNA alone or ascorbic acid alone, no DNA cleavage is observed. The concentration-dependent DNA clea-vage experiments were carried out for **1**, **2**, and **4** with a constant concentration of DNA (40 μM in base pairs) and ascorbic acid (30 μM). It is clearly seen that **1** and **2** effect efficient DNA cleavage at 30 μM (NC DNA, 96%) and 20 μM (NC DNA, 90%) concentrations, respectively (Figure S5A in the Supporting Information), while **4** cleaves DNA completely (100%) even at 6 μM concentration (Figure S5B in the Supporting Infor-mation). As the concentration of **4** is increased, the amount of NC DNA (form II) increases, reaches a maximum (complete conversion) at nearly 6 μM, and remains constant until 8 μM (Figure S5B in the Supporting Information), where the linear

Table 5. Concentration-Dependent DNA Cleavage Data of SC pUC19 DNA (40 μM in Base Pairs) by Complex 4 in the Absence of External Agent

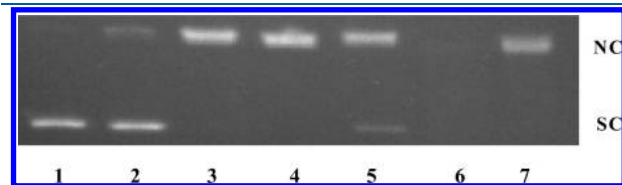| serial no.	reaction conditions	form (%)	
		SC	NC
1	DNA control	89.1	10.9
2	DNA + **4** (10 μM)	75.1	24.9
3	DNA + **4** (20 μM)	86.8	13.2
4	DNA + **4** (30 μM)	50.8	49.2
5	DNA + **4** (40 μM)	32.4	67.6
6	DNA + **4** (80 μM)	4.4	95.6
7	DNA + **4** (100 μM)	8.3	91.7
8	DNA + **4** (120 μM)	11.2	88.8
9	DNA + **4** (160 μM)	8.0	92.0

Figure 7. DNA cleavage of SC pUC19 DNA (40 μM) by copper(II) complexes in a buffer containing a 5% DMF buffer in the presence of ascorbic acid (H$_2$A) at 37 °C: lane 1, DNA control; lane 2, DNA + H$_2$A; lane 3, DNA + H$_2$A + **1**; lane 4, DNA + H$_2$A + **2**; lane 5, DNA + H$_2$A + **3**; lane 6, DNA + H$_2$A + **4**; lane 7, DNA + H$_2$A + $[Cu(dpq)_2]^+$. The complex concentration is 30 μM for lanes 3−7. SC and NC are supercoiled and nicked-circular forms of DNA, respectively.
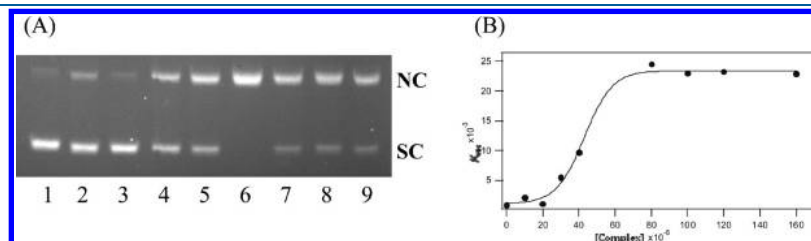
Figure 6. (A) Concentration-dependent cleavage of SC pUC19 (40 μM in base pairs) with different concentrations of complexes: lane 1, DNA; lane 2, DNA + **4** (0.01 mM); lane 3, DNA + **4** (0.02 mM); lane 4, DNA + **4** (0.03 mM); lane 5, DNA + **4** (0.04 mM); lane 6, DNA + **4** (0.08 mM); lane 7, DNA + **4** (0.1 mM); lane 8, DNA + **4** (0.12 mM); lane 9, DNA + **4** (0.16 mM). SC and NC are supercoiled and nicked-circular forms of DNA, respectively. (B) Plot of complex concentrations against the rate of DNA cleavage.

Table 6. Oxidative Cleavage Data of SC pUC19 DNA (40 μM in Base Pairs) by Complexes 1−4 (30 μM) in the Presence of Ascorbic Acid (10 μM) for an Incubation Time of 1 h

		form %	
serial no.	reaction conditions	SC	NC
1	DNA control	90.6	9.4
2	DNA + H$_2$A	89.8	10.2
3	DNA + H$_2$A + **1**	3.0	97.0
4	DNA + H$_2$A + **2**	2.0	98.0
5	DNA + H$_2$A + **3**	8.0	92.0
6	DNA + H$_2$A + **4**	a	a
7	DNA + H$_2$A + [Cu(dpq)$_2$(H$_2$O)](ClO$_4$)$_2$	2.0	98.0

^{a} Completely degraded.

Table 7. Oxidative Cleavage Data of SC pUC19 DNA (40 μM in Base Pairs) by Complexes 1−4 (10 μM) in the Presence of H$_2$O$_2$ (200 μM) for an Incubation Time of 1 h

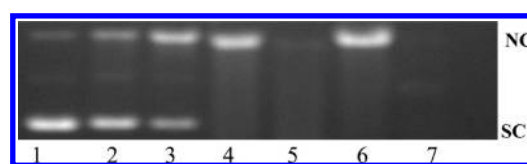|		form %	
serial no.	reaction conditions	SC	NC
1	DNA control	92.6	7.4
2	DNA + H$_2$O$_2$	86.0	14.0
3	DNA + H$_2$O$_2$ + **1**	45.0	55.0
4	DNA + H$_2$O$_2$ + **2**	2.0	98.0
5	DNA + H$_2$O$_2$ + **3**	a	a
6	DNA + H$_2$O$_2$ + **4**	4.0	96.0
7	DNA + H$_2$O$_2$ + [Cu(dpq)$_2$(H$_2$O)](ClO$_4$)$_2$	a	a

^{a} Completely degraded.

form of DNA (form III) is not observed at all under the present conditions. This suggests that DNA cleavage occurs randomly because a significant portion of plasmid DNA is already converted to the NC form without concurrent formation of the SC form. Above a 8 μM concentration, DNA is degraded completely. The (100%) DNA cleavage efficiency shown by complex **4** (6 μM) is higher than its corresponding Cu(dpq)$^{2+}$,[60] Cu-(dpq)$_2$$^{2+}$,[61] and [Cu(dpq)$_3$]$^{2+}$[36] complexes. The high affinity of **4** for intercalative DNA binding could be related to the presence of an extended aromatic ring of the dpq ligand, making noncovalent interactions between the π system of the ligands and DNA base pairs more favorable in association with the close proximity of the phenolato bridge, which enhances the nuclease ability of dinuclear complexes.[26−32] Also, it has been reported that the Cu(bpy)$^{2+}$,[60] Cu(bpy)$_2$$^{2+}$,[61] and mixed-ligand copper-(II)[25] complexes containing bpy as the coligand are nuclease-inactive. However, it is interesting that the bpy complex **1** shows complete conversion of SC DNA into NC DNA at a 30 μM complex concentration. The prominent DNA cleavage exhibited by **4** suggests that DNA binding in the form of partial intercalation could be an important factor for the cleavage activity. It is likely that generation of a hydroxyl radical and/or activated oxygen mediated[57] by the copper(II) complexes results in DNA cleavage.

The mechanism of pUC19 DNA cleavage by all of the four complexes was studied by the addition of the hydroxyl radical inhibitor DMSO (Figure S6 in the Supporting Information). It was found that the addition of DMSO significantly diminishes the nuclease activity, indicating the involvement of the hydroxyl radical in the cleavage process. The complexes would first interact with DNA by intercalation to form a Cu^{II}DNA adduct species followed by its reduction by the added reductant to a Cu^{I}DNA adduct, which then generates hydroxyl radicals by reaction with ^{3}O$_2$. These hydroxyl radicals would then attack DNA, causing strand scission. Also, it is observed that among all of the complexes only the 5,6-dmp complex exhibits DNA cleavage in the presence of a minor groove binder like distamycin, which reveals that the 5,6-dmp complex alone binds to the DNA major groove to cleave DNA and all of the remaining complexes cleave DNA after binding to the DNA minor groove. On the basis of all of these results, we propose that the complex interacts with DNA through the minor groove, after which the copper(II) centers are reduced in the presence of an activating agent to copper(I) species. The latter subsequently reacts with O$_2$ to give rise to the hydroxyl radicals needed for DNA breakdown.

Figure 8. DNA cleavage of SC pUC19 DNA (40 μM) by copper(II) complexes in a buffer containing 5% DMF/5 mM Tris HCl and 50 mM NaCl in the presence of H$_2$O$_2$ at 37 °C: lane 1, DNA control; lane 2, DNA + H$_2$O$_2$; lane 3, DNA + H$_2$O$_2$ + **1**; lane 4, DNA + H$_2$O$_2$ + **2**; lane 5, DNA + H$_2$O$_2$ + **3**; lane 6, DNA + H$_2$O$_2$ + **4**; lane 7, DNA + H$_2$O$_2$ + [Cu(dpq)$_2$]$^+$. The complex concentration is 10 μM for lanes 3−7. SC and NC are supercoiled and nicked-circular forms of DNA, respectively.

The ability of **1**−**4** to cause DNA cleavage (10 μM) in a 5% DMF/5 mM Tris-HCl/50 mM NaCl buffer at pH 7.1 has also been studied in the presence of H$_2$O$_2$ (200 μM) as an activator by gel electrophoresis using SC pUC19 DNA (40 μM in base pairs) after incubation of the reaction mixture at 37 °C for 1 h. At 10 μM complex concentration, conversion of DNA from the SC form to the NC form is observed. While **2** and **4** cause respectively 98% and 96% DNA cleavage (Table 7), **1** exhibits only 55% DNA cleavage. For **3**, interestingly, complete degradation of SC DNA to undetectable smaller fragments is observed (Figure 8). In the control experiment with DNA alone and DNA with H$_2$O$_2$, no cleavage is observed. Because **2**−**4** exhibit efficient cleavage activity in the presence of H$_2$O$_2$ under identical conditions, they were subjected to concentration-dependent cleavage studies. As the complex concentration is increased, the disappearance of form I and appearance of form II are observed. At concentrations of 2 and 5 μM, respectively, complexes **2** and **4** exhibit more than 90% DNA cleavage (Figure S7A,B and Tables S4 and S5 in the Supporting Information); however, interestingly, **3** displays the same percentage of DNA cleavage even at 0.2 μM (200 nM) concentration (Figure 9 and Table 8), and the smaller fragments of undetectable DNA are observed at 10 μM complex concentration. It is known that copper(II) complexes interact with DNA in the presence of O$_2$ or a redox agent, the ROS generated, causing major DNA damage.[62−65] When the standard radical scavenger DMSO is added to the reaction mixture, a dramatic reduction in DNA cleavage is observed. Also, upon the addition of NaN$_3$ (singlet oxygen quencher) to the reaction mixture, the cleavage reaction is inhibited significantly. Further, the 5,6-dmp complex **3** shows DNA cleavage more efficient
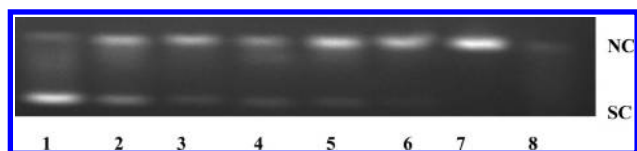
6464

dx.doi.org/10.1021/ic1024185 |*Inorg. Chem.* 2011, 50, 6458–6471

Figure 9. Concentration-dependent DNA (20 μM) cleavage by complex **3** (0.05–10 μM) in 5% DMF/5 mM Tris-HCl/50 mM NaCl at pH 7.1 and 37 °C in the presence of H_2O_2 (200 μM) at 37 °C: lane 1, DNA + H_2O_2; lane 2, DNA + H_2O_2 + **3** (0.05 μM); lane 3, DNA + H_2O_2 + **3** (0.1 μM); lane 4, DNA + H_2O_2 + **3** (0.2 μM); lane 5, DNA + H_2O_2 + **3** (0.5 μM); lane 6, DNA + H_2O_2 + **3** (1 μM); lane 7, DNA + H_2O_2 + **3** (5 μM); lane 8, DNA + H_2O_2 + **3** (10 μM). Forms I and II are supercoiled and nicked-circular forms of DNA, respectively.

Table 8. Concentration-Dependent Oxidative Cleavage Data of SC pUC19 DNA (40 μM in Base Pairs) by Complex 3 in the Presence of H_2O_2 (200 μM)

serial no.	reaction conditions	form (%) SC	form (%) NC
1	DNA + H_2O_2	86.3	13.7
2	DNA + H_2O_2 + **3** (0.05 μM)	14.0	86.0
3	DNA + H_2O_2 + **3** (0.10 μM)	12.0	88.0
4	DNA + H_2O_2 + **3** (0.20 μM)	10.0	90.0
5	DNA + H_2O_2 + **3** (0.50 μM)	6.0	94.0
6	DNA + H_2O_2 + **3** (1.00 μM)	4.0	96.0
7	DNA + H_2O_2 + **3** (5.00 μM)	2.0	98.0
8	DNA + H_2O_2 + **3** (10.0 μM)	[a]	[a]

[a] Completely degraded.

than the phen (**2**) and dpq (**4**) complexes, both bound to DNA through partial intercalation, as is bound to the surface of DNA in the major groove. It is also possible that the copper(I) species produced would interact with H_2O_2 to generate hydroxyl radicals (Fenton mechanism).[66] The above mechanism of DNA cleavage mediated by the complexes is similar to that proposed for other di- and multinuclear copper(II) complexes.[31,32] Thus, all of the complexes exhibit DNA cleavage activity with an activator like ascorbic acid or H_2O_2, which plays a vital role in determining the type of DNA cleavage observed without an activator and also supports the proposed mechanisms of cleavage involving •OH radicals.

Studies on the Anticancer Activity of Complexes. The cytotoxicity of the strongly DNA binding and cleaving complexes **1–4** on HEp-2 human larynx cancer cell line has been evaluated in comparison with the widely used drug cisplatin under identical conditions by using MTT assay. The IC_{50} values determined (1.3 ± 0.1–29.4 ± 4.3 μM at 24 h and 0.79 ± 0.10–22.4 ± 3.7 μM at 48 h; Table 9) are found to be significant, and they follow the trend **1 > 2 > 4 > 3**. This clearly indicates that the anticancer activity of the complexes is time-dependent and varies with the mode and extent of their interaction with DNA. The IC_{50} values determined for the free coligands (Table 9) are 9–40 times higher than those for the respective complexes, revealing that the complex species rather than the dissociated coligands are actually responsible for the observed antitumor activity of the complexes. While **2** and **4** exhibit appreciable cytotoxic effects, **3** is remarkable in displaying a cytotoxic effect (IC_{50}, 0.79 ± 0.10 μM) approximately 10 times more prominent than that

Table 9. In Vitro Cytotoxicity Assays for Complexes 1–4 and Ligands against HEp-2 Human Larynx Cancer Cell Line (IC_{50} Values in Millimolar Concentration)

complex/ligand	[a]IC_{50} (μM) 24 h	[a]IC_{50} (μM) 48 h
$[Cu_2(LH)_2(bpy)_2(ClO_4)_2]^{2+}$ (**1**)	29.4 ± 4.3	22.4 ± 3.7
$[Cu_2(LH)_2(phen)_2(ClO_4)_2]^{2+}$ (**2**)	4.3 ± 0.5	9.6 ± 0.4
$[Cu_2(LH)_2(5,6\text{-dmp})_2(ClO_4)_2]^{2+}$ (**3**)	1.3 ± 0.1	0.8 ± 0.1
$[Cu_2(LH)_2(dpq)_2(ClO_4)_2]^{2+}$ (**4**)	4.5 ± 0.3	3.1 ± 0.2
bpy	<250	<200
phen	<200	185.5 ± 10.0
5,6-dmp	43.0 ± 5.0	32.4 ± 3.0
dpq	123.5 ± 12.4	94.3 ± 12.2

[a] IC_{50} = concentration of the drug required to inhibit growth of 50% of the cancer cells (in μM).

of cisplatin (IC_{50}, 7.1 ± 2.7 μM).[67] It is evident that the hydrophobic forces of interaction of the 5,6-dmp complex **3** lead to its highest cytotoxicity. We have obtained similar results for the mixed-ligand complexes $[Cu(\text{L-tyr})(5,6\text{-dmp})]^{+25}$ and $[Cu(tdp)(tmp)]^+$ [tmp = 3,4,7,8-tetramethyl-1,10-phenanthroline; H(tdp) = 2-[(2-(2-hydroxyethylamino)(ethylimino)-methyl]phenol],[21] which exhibit stronger DNA binding through hydrophobic forces of interaction involving 5,6-dmp and tmp coligands and show percentages of apoptosis cell death higher than those of their bpy, phen, and dpq analogues. Because the cell killing activity of the copper(II) complexes is similar to that of cisplatin,[68] the present complexes are suitable candidates for potential applications as anticancer drugs.

Apoptosis (programmed cell death) is a normal component of the development and maintenance of health of multicellular organisms. Cells die in response to a variety of external and physiological stimuli, and during apoptosis, they do so in a controlled and regulated fashion. This makes apoptosis distinct from the other form of cell death, called necrosis, in which uncontrolled (accidental) cell death leads to lysis of cells, to inflammatory responses, and, potentially, to serious health problems. Also, apoptosis, by contrast, is a process in which cells play an active role in their own death (cell suicide). Most tumor cells retain their sensitivity to some apoptotic stimuli from chemotherapeutic agents, and in this context, the apoptosis-inducing ability of drugs seems to be a primary factor in determining their efficacy.[69] To understand the mode of cell death caused by **3**, we have employed different biochemical techniques like fluorescent staining for morphological assessment, single-cell gel electrophoresis (comet assay) for detecting DNA fragmentation, mitochondrial membrane potential ($\Delta\Psi_m$) to assess changes in the membrane potential, and a Western blotting technique to evaluate the expression level of the pro- and antiapoptotic proteins.

Fluorescent Staining Method. The characteristic morphological changes induced by **3** have been evaluated by adopting fluorescent microscopic analysis of Hoechst 33258- and acridine orange/EthBr (AO/EB)-stained cells (Figure 10). The results obtained reveal that the complexes induce cell death through different modes like apoptosis and necrosis. Upon treatment of the cells with IC_{50} concentration of **3** at different incubation times (24 and 48 h), morphological changes such as chromatin fragmentation, bi- and/or multinucleation, cytoplasmic vacuolation, nuclear swelling, cytoplasmic blebbing, and late apoptosis
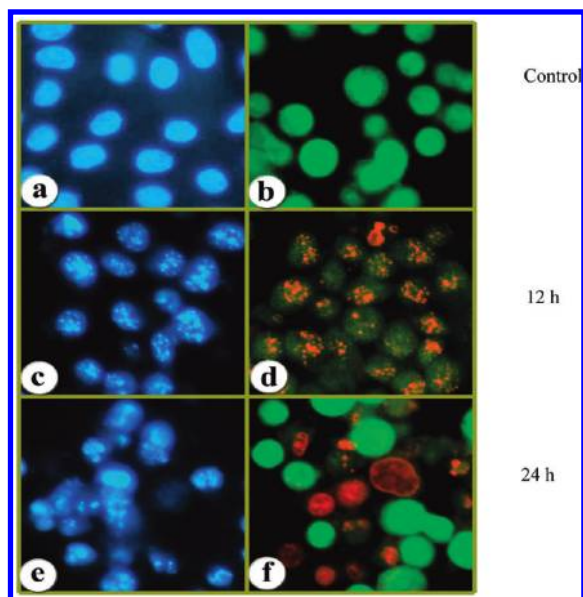
Figure 10. AO/EB- and Hoechst 33258-stained HEp-2 human larynx cancer cells: (a and b) untreated cells; (c and d) at 24 h and (e and f) at 48 h incubation by the treatment of **3**.

Figure 11. Comet assay of EB-stained (a) control (untreated) **3** and (b and c) treated cells.

Figure 12. (A) Mitochondrial trans membrane potency of complex **3**: control (a) (untreated) and treated with **3** (b and c) at different times of incubation. (B) Schematic representation of major stimuli for the induction of apoptosis.[72].

indication of dotlike chromatin condensation[70] have been observed by adopting Hoechst 33258 staining. The cytological changes observed are classified into four types according to the fluorescence emission and morphological features of chromatin condensation in the AO/EB-stained nuclei: (i) viable cells having uniformly green fluorescing nuclei with highly organized structure; (ii) early apoptotic cells (which still have intact membranes but have started undergoing DNA fragmentation) having green fluorescing nuclei but with perinuclear chromatin condensation visible as bright-green patches or fragments; (iii) late apoptotic cells having orange-to-red fluorescing nuclei with condensed or fragmented chromatin; (iv) necrotic cells, swollen to large sizes, having uniformly orange-to-red fluorescing nuclei with no indication of chromatin fragmentation. All of these morphological changes indicate that the cells are committed to death in such a way that both apoptotic and necrotic cells increase in number in a time-dependent manner. The apoptotic morphologies induced by **3** are confirmed by AO/EB staining adopting fluorescence microscopy, which suggests that the complex causes apoptosis more efficiently than all other complexes during 24 and 48 h treatment, and the percentage of the apoptotic mode of cell death caused at 48 h is higher than that at 24 h. Similar observations have been made by us for the mixed-ligand complexes [Cu-(tdp)(tmp)]$^{+2}$[21] and [Cu(L-tyr)(5,6-dmp)]$^{+}$,[25] which show a percentage of apoptosis cell death higher than that of their other phen analogues.

Single-Cell Gel Electrophoresis. The single-cell gel electrophoresis (comet) assay has also been used to evaluate single- and double-stranded DNA breaks at the single-cell level because the assay detects DNA breaks, alkali-labile lesions, and genomic lesions that are subject to DNA repair.[71] When the cancer cells are treated with IC$_{50}$ concentration of **3**, statistically significant and well-formed comets are observed, while the control (untreated) cells fail to show a cometlike appearance (Figure 11). This clearly reveals that the complex indeed induces DNA fragmentation, which is a hallmark of apoptosis.[71] The high levels of DNA damage induced by the complex reinforces the
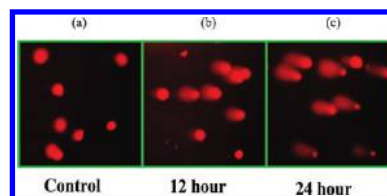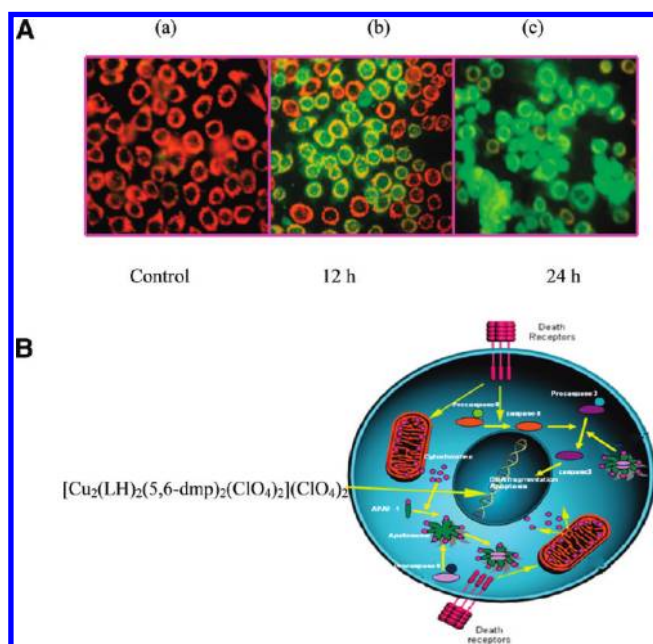
above results obtained by using MTT assay and fluorescent staining assay.

Apoptosis Detection by Mitochondrial Membrane Potential ($\Delta\Psi_m$) Analysis. In this analysis, the mitochondrial membrane potential is monitored using JC1, a cell-permeable fluorescent dye, which preferentially enters into mitochondria because of the highly negative mitochondrial membrane potential and confers a green fluorescence. It is well-known that, upon a loss of the membrane integrity, the mitochondrial potential changes, cytochrome *c* located normally inside the mitochondria is translocated into the cytosol, and the JC1 dye is released from mitochondria, which leads to a decrease in the intracellular fluorescence (Figure 12A). The cancer cells were treated with **3** at different incubation time intervals to understand the effect of the complex on the mitochondrial membrane potential and, hence, the translocation of cytochrome *c*. With an increase in time, the intracellular fluorescence is found to decrease, revealing an increase in the loss of membrane potential and leading to the release of cytochrome *c*. The cytochrome *c* released binds with apaf1 protein to form an apotosome complex and activates the cascades of caspase proteins, which triggers the enzymes and proteins to cause DNA fragmentation, leading to apoptosis. Thus, the observed loss of fluorescence by the cancer cells upon

treatment with **3** clearly reveals that the complex induces apoptosis in cancer cells via the mitochondrial pathway, that is, release of cytochrome c from mitochondria to cytosol, leading to caspase activation during the apoptotic process. Some of the major stimuli that can induce apoptosis are illustrated in Figure 12B.[72]

Western Blotting Analysis. The tumor suppressor protein p53 is a redox-active transcription factor that coordinates and prepares cellular mechanisms in response to a variety of stresses that lead to genomic instability. It occupies a pivotal role in maintaining the genomic integrity[72] because it plays a vital role in cell arrest, DNA repair, cellular senescence, differentiation, and apoptosis. It also facilitates the repair and survival of scarcely damaged cells and eliminates severely damaged cells from the replicative pool to protect the organism. Also, both proteins Bcl-2 and Bax are transcriptional targets for p53, which induces apoptosis in response to DNA damage.[73] It is widely accepted that these three proteins are very important in deciding the issues of cell suicide.[74] Now, the expression of the proapoptotic p53 and Bax and antiapoptotic Bcl-2 proteins in HEp-2 larynx cancer cell lines treated for 24 and 48 h with **3** has been determined, and the results obtained are referenced to a control experiment (without drug treatment). It is found that the expression level of the Bcl-2 protein decreases and the Bax protein level is constitutively expressed, suggesting that apoptosis by **3** could be mediated through the downregulation of the antiapoptotic protein Bcl-2 (Figure S8 in the Supporting Information). However, as shown in Figure S8 in the Supporting Information, the p53 protein level in HEp-2 larynx cancer cell lines is markedly increased upon treatment with **3** in a time-dependent manner (increase in the level of the expression of the p53 status in the presence of **3**), revealing that the complex induces apoptosis by activating the p53 apoptosis pathway. The p53 protein is activated in response to DNA damage, which subsequently unbalances the Bax/Bcl-2 ratio. The Bcl-2 family of proteins regulates apoptosis by controlling the mitochondrial permeability and the release of cytochrome c. The expression level of antiapoptotic protein Bcl-2 is a critical intracellular checkpoint of apoptosis within a distal common cell death pathway. It is stated that the main mechanism for apoptosis appears to be a mitochondria-mediated pathway accompanied by loss of the mitochondrial transmembrane potential (cf. above) followed by cytochrome c release from mitochondria into cytosol, resulting in activation of caspase cascades and leading to apoptosis.[75] Also, the upregulation of proapoptotic protein p53 and the downregulation of antiapoptotic protein Bcl-2 caused by **3** could possibly activate mitochondria-mediated apoptosis.

It is expected that the DNA groove-binding complex **3** with hydrophobic 5,6-dmp coligand, which exists as the dicationic $[Cu_2(LH)_2(5,6\text{-dmp})_2(ClO_4)_2]^{2+}$ species (cf. above), would adhere to the plasma membrane by electrostatic attraction, get transported across the cell membrane by a concentration gradient, and then interfere with the cellular function of DNA by binding to it. Thus, the prominent cytotoxicity of the 5,6-dmp complex is consistent with its strong DNA binding affinity and efficient DNA cleavage in the presence of H_2O_2. Also, a complex like **4** with a higher DNA binding affinity and DNA cleavage ability fails to show cytotoxicity higher than its DNA groove-binding analogue **3**. The complexes might exhibit cytotoxicity by inducing apoptosis, which plays a key role in regulating the cell cycle. So, if the drug is to exhibit cytotoxicity by inducing apoptosis, it should target and inhibit some of the proteins

involved in the cancer profile. The above MTT assay and morphological changes observed reveal that the 5,6-dmp complex possesses a very prominent cytotoxicity.

■ CONCLUSIONS

The mixed-ligand dinuclear copper(II) complexes of bpy, phen, 5,6-dmp, and dpq exhibit prominent DNA cleavage in the presence of activators, which is higher than those of their corresponding mono- and bis(diimine) complexes. The minor groove-bound dpq complex completely degrades SC DNA into undetectable smaller fragments even at 8 μM concentration and shows an oxidative DNA cleavage in the absence and presence of the activator ascorbic acid with efficiency more profound and prominent than that of the other diimine complexes. So, it is evident that the partially intercalating coligand dpq is an excellent DNA recognition element, which could be used to design robust and efficient copper(II)-based chemical nucleases. On the other hand, the 5,6-dmp complex preferentially docked in the DNA major groove behaves as a chemical nuclease even at a lower complex concentration of 0.2 μM in the presence of H_2O_2 as an activator with efficiency higher than that of the other complexes. Thus, the DNA binding behavior and, hence, the DNA cleavage efficiency of the mixed-ligand dinuclear copper(II) complexes are dictated by the size, shape, and electronic structures of the dinuclear copper(II) complexes, as determined by the diimine coligands. Also, while the diimine ligand could function as a DNA recognition element, the amide group of the primary ligand and/ or a water molecule present in the axial copper site could promote DNA binding and DNA cleavage.

The dinuclear copper(II) complexes with phen, 5,6-dmp, and dpq coligands exhibit anticancer activities toward human larynx cancer cell lines (HEp-2) more potent than the widely used drug cisplatin. This reveals that a synergic combination of the ligand and metal ion is important in the design of a potential anticancer drug, the activity of which correlates well with the ability of the complexes to strongly bind and cleave DNA. Thus, the hydrophobic forces of interaction exhibited by the 5,6-dmp ligand, which is responsible for the stronger DNA groove binding, more effective DNA cleavage of the complex in the presence of H_2O_2 as an activator, and more facile transport across the cell membrane of the hydrophobic 5,6-dmp complex, account for the enhanced cytotoxicity of the complex. Also, biochemical studies like fluorescence staining, comet assay, mitochondrial transmembrane potential, and Western blotting technique reveal that the 5,6-dmp complex acts as a potent anticancer agent by inducing phenotypical changes, DNA fragmentation, loss of mitochondrial membrane potential, and upregulation of proapoptotic proteins or downregulation of antiapoptotic proteins, which is consistent with the induction of mainly apoptotic cell death. Thus, it emerges from the present study that the water-soluble 5,6-dmp complex can act as an efficacious antiproliferative drug by inducing morphological changes consistent with the induction of apoptotic cell death. Further mechanistic and cellular uptake studies are essential to probe the higher potency of the complex to kill cancer cells.

■ EXPERIMENTAL SECTION

Reagents and Materials. Copper(II) perchlorate hexahydrate (Aldrich), 1,10-phenanthroline (Merck, India), calf thymus (CT) DNA (highly polymerized stored at 4 °C), superoxide dismutase (SOD),

6467

dx.doi.org/10.1021/ic1024185 |*Inorg. Chem.* 2011, 50, 6458–6471

catalase (Sigma, stored at −20 °C), and plasmid SC pUC19 DNA and agarose (Genei, Bangalore, India) were used as received. Ultrapure Milli-Q water (18.2 MΩ) was used in all experiments. The ligand dipyrido-[3,2-d:2′,3′-f]quinoxaline (dpq)[35] and ligand 2-hydroxy-N-[2-(methyl-amino)ethyl]benzamide (LH)[76] were prepared by their reported procedure. The commercial solvents were distilled and then used for the preparation of complexes.

HEp-2 human larynx cancer cell line was obtained from National Center for Cell Science, Pune, India. The cells were cultured in a RPMI 1640 medium (Biochrom AG, Berlin, Germany), supplemented with 10% fetal bovine serum (Sigma, Madison, WI), in 96-well culture plates, at 37 °C in a humidified atmosphere of 5% CO_2 in a CO_2 incubator (Heraeus, Hanau, Germany). All of the experiments were performed using cells from passage 15 or less.

Synthesis of LH. To a methanolic solution of N-methylethylenediamine (0.9 mL, 10 mmol) and 1-methylsalicylate (1.3 mL, 10 mmol) was added 20 mL of acetonitrile. The resulting solution was stirred for 12 h. The colorless crystalline product obtained was filtered off and washed with water and then ether.[76] The crude product was recrystallized from ethanol to give a crystalline product. MP: 138 °C. ^{1}H NMR (200 MHz, CDCl$_3$): δ 7.6−6.9 (m, 4H), 6.8 (s, 1H), 3.4 (t, 2H), 2.9 (t, 2H), 2.3 (s, 1H), 2.1 (s, 3H).

Isolation of 1. A methanolic solution (5 mL) of copper(II) perchlorate hexahydrate (0.37 g, 1 mmol) was added to a solution of LH (0.19 g, 1 mmol) in methanol (5 mL) with constant stirring. Then a solution of 2,2′-bipyridine (0.15 g, 1 mmol) in methanol (5 mL) was added to the reaction mixture with constant stirring. The dark-green complex was filtered off and dried under vacuum. The concentrated methanolic solution of complex **1** kept aside for 1 week. By the slow evaporation of solution, green crystals were obtained. Anal. Calcd for $C_{40}H_{44}Cl_4Cu_2N_8O_{20}$: C, 39.2; H, 3.62; N, 9.14. Found: C, 39.18; H, 3.6; N, 9.12. ESI-MS: $\{[Cu_2(LH)_2(bpy)_2(ClO_4)_2](ClO_4)\}^+$ displays a peak at m/z 1124.53 (calcd m/z 1123.07).

Isolation of $[Cu_2(LH)_2(phen)_2(ClO_4)_2](ClO_4)_2$ (2). A methanolic solution (5 mL) of copper(II) perchlorate hexahydrate (0.37 g, 1 mmol) was added to a solution of LH (0.19 g, 1 mmol) in methanol (5 mL) with constant stirring. During stirring, a solution of 1,10-phenanthroline (0.19 g, 1 mmol) in methanol (5 mL) was added. The dark-green precipitate obtained was filtered off and dried under vacuum. Anal. Calcd for $C_{44}H_{44}Cl_4Cu_2N_8O_{20}$: C, 41.49; H, 3.48; N, 8.8. Found: C, 41.5; H, 3.49; N, 8.82. ESI-MS: $\{[Cu_2(LH)_2(phen)_2(ClO_4)_2](ClO_4)\}^+$ displays a peak at m/z 1171.07 (calcd m/z 1171.60).

Isolation of $[Cu_2(LH)_2(5,6\text{-}dmp)_2(ClO_4)_2](ClO_4)_2$ (3). A methanolic solution (5 mL) of copper(II) perchlorate hexahydrate (0.37 g, 1 mmol) was added to a solution of LH (0.19 g, 1 mmol) in methanol (5 mL). To the reaction mixture was added a methanolic solution (5 mL) of 5,6-dimethyl-1,10-phenanthroline (0.21 g, 1 mmol). The green complex obtained was filtered off and washed with diethyl ether. Anal. Calcd for $C_{48}H_{52}Cl_4Cu_2N_8O_{20}$: C, 43.35; H, 3.94; N, 8.43. Found: C, 43.37; H, 3.95; N, 8.45. ESI-MS: $\{[Cu_2\text{-}(LH)_2(5,6\text{-}dmp)_2(ClO_4)_2](ClO_4)\}^+$ displays a peak at m/z 1227.14 (calcd m/z 1130.53).

Isolation of $[Cu_2(LH)_2(dpq)_2(ClO_4)_2]_2(ClO_4)_2$ (4). A methanolic solution (5 mL) of copper(II) perchlorate hexahydrate (0.37 g, 1 mmol) was added to a solution of LH (0.19 g, 1 mmol) in methanol (5 mL) with constant stirring. The color of the solution changed to green. Then a solution of dpq[32] (0.23 g, 1 mmol) in methanol (5 mL) was added with constant stirring. The green complex was filtered off and dried under vacuum. Anal. Calcd for $C_{48}H_{44}Cl_4Cu_2N_{12}O_{20}$: C, 41.84; H, 3.22; N, 12.2. Found: C, 41.85, H, 3.25, N, 12.2.

Methods and Instruments. Microanalyses (C, H, and N) were carried out with a Vario EL elemental analyzer. UV−visible spectroscopy was recorded on a Varian Cary 300 Bio UV−visible spectrophoto-

meter using cuvettes of 1 cm path length. Emission intensity measurements were carried out using a Jasco F 6500 spectrofluorimeter. Viscosity measurements were carried out using a Schott Gerate AVS 310 automated viscometer.

Solutions of DNA in the buffer 5 mM Tris HCl/50 mM NaCl in water gave a ratio of UV absorbance at 260 and 280 nm, A_{260}/A_{280}, of 1.9,[77] indicating that the DNA was sufficiently free of protein. Concentrated stock solutions of DNA (16.5 mM) were prepared in a buffer and sonicated for 25 cycles, where each cycle consisted of 30 s with 1 min intervals. The concentration of DNA in nucleotide phosphate (NP) was determined by UV absorbance at 260 nm after 1:100 dilutions. The extinction coefficient, ε_{260}, was taken as 6600 M^{-1} cm^{-1}. Stock solutions were stored at 4 °C and used after no more than 4 days. Plasmid SC pUC19 DNA was stored at −20 °C, and the concentration of DNA in base pairs was determined by UV absorbance at 260 nm after appropriate dilutions taking ε_{260} as 13 100 M^{-1} cm^{-1}. Concentrated stock solutions of metal complexes were prepared by dissolving calculated amounts of metal complexes in the respective amount of solvent and diluted suitably with a corresponding 5% DMF/5 mM Tris-HCl/50 mM NaCl buffer at pH 7.1 to the required concentrations for all of the experiments.

X-ray Crystallography. A crystal of suitable size was selected from the mother liquor, immersed in paraffin oil, then mounted on the tip of a glass fiber, and cemented using epoxy resin. Intensity data for the crystal were collected using Mo Kα (λ = 0.710 73 Å) radiation on a Bruker SMART APEX diffractometer equipped with a CCD area detector at 293 K. The crystallographic data are collected in Table 1. The SMART program[78] was used for collecting frames of data, indexing reflections, and determining lattice parameters; the SAINT[79] program for integration of the intensity of reflections and scaling, the SADABS[80] program for absorption correction, and the SHELXTL[81] program for space group and structure determination and least-squares refinements on F^2. The structure was solved by a heavy-atom method. The non-hydrogen atoms were located in successive difference Fourier syntheses. The final refinement was performed by full-matrix least-squares analysis. Hydrogen atoms attached to the ligand moiety were located from the difference Fourier map and refined isotropically.

DNA Binding and Cleavage Experiments. Concentrated stock solutions of metal complexes were prepared by dissolving them in a 5% DMF/5 mM Tris-HCl/50 mM NaCl buffer at pH 7.1 of metal complexes and diluting suitably with the corresponding buffer to the required concentrations for all of the experiments. For absorption and emission spectral experiments, the DNA solutions were pretreated with solutions of metal complexes to ensure no change in the concentration of the metal complexes.

Absorption spectral titration experiments were performed on a Varian Cary 300 Bio UV−visible spectrophotometer by maintaining a constant concentration of the complex while varying the nucleic acid concentration. This was achieved by dissolving an appropriate amount of the complex and DNA stock solutions while maintaining the total volume constant (1 mL). This results in a series of solutions with varying concentrations of DNA but with a constant concentration of the complex. The absorbance (A) of the most red-shifted band of each investigated complex was recorded after successive additions of CT DNA.

Emission intensity measurements were carried out using a 5% DMF/5 mM Tris-HCl/50 mM NaCl buffer solution as a blank to make preliminary adjustments. The excitation wavelength was fixed and the emission range was adjusted before measurements. DNA was pretreated with EthBr in the ratio [DNA/EthBr] = 10 for 30 min at 27 °C. The metal complexes were then added to this mixture, and their effect on the emission intensity was measured.

For viscosity measurements, the Schott Gerate AVS 310 automated viscometer was thermostatted at 25 °C in a constant-temperature bath. The concentration of DNA was 500 μM in NP, and the flow

times were noted from the digital timer attached with the viscometer ($1/R = [\text{Cu}]/[\text{DNA}] = 0.5$).

The cleavage of DNA in the absence and presence of activating agents like ascorbic acid (10 μM) or H$_2$O$_2$ (200 μM) was monitored using agarose gel electrophoresis. Reactions using plasmid SC pUC19 DNA (form I, 40 μM) in a 5% DMF/5 mM Tris-HCl/50 mM NaCl buffer at pH 7.1 were treated with copper complexes. The cleavage of DNA in the absence of activating agents was monitored using agarose gel electrophoresis. The samples were incubated for 1 h at 37 °C. A loading buffer containing 25% bromophenol blue, 0.25% xylene cyanol, and 30% glycerol (3 μL) was added and electrophoresis performed at 60 V for 5 h in a tris-acetate-EDTA (TAE) buffer (40 mM tris-base, 20 mM acetic acid, and 1 mM EDTA) using 1% agarose gel containing 1.0 μg/mL EthBr. The gels were viewed in a Alpha Innotech Corp. gel doc system and photographed using a CCD camera. Densitometric calculations were made using the AlphaEaseFC Stand Alone software. The intensities of SC DNA were corrected by a factor of 1.47 as a result of its lower staining capacity by EthBr.[82] The cleavage efficiency was measured by determining the ability of the complex to convert DNA from the SC form to the NC form.

The decrease in the intensities of form I (SC), or the increase in the intensities of form II (NC), was then plotted against catalyst concentrations, and these were fitted well with a single-exponential decay curve (pseudo-first-order kinetics) by the use of known equations.[55] For anaerobic experiments, deoxygenated water and anaerobic stock solutions were prepared. In order to identify the ROS involved in the cleavage reaction, the radical scavengers such as the hydroxyl radical (DMSO, 10%), singlet oxygen (NaN$_3$, 100 μM), SOD (10 unit), and H$_2$O$_2$ (catalase, 0.1 unit) were introduced. The reaction products were resolved on 1% agarose gel in a TAE buffer.

Cell Viability Assay. MTT assay was carried out as described previously.[83] Complexes **1**−**4**, in the concentration range of 0.05−50 μM, dissolved in H$_2$O were added to the wells 24 h after seeding of 5×10^3 cells well^{-1} in 200 μL of a fresh culture medium. After 24 and 48 h, 20 μL of a MTT solution [5 mg/mL in phosphate-buffered saline (PBS)] was added to each well, and the plates were wrapped with aluminum foil and incubated for 4 h at 37 °C. The purple formazan product was dissolved by the addition of 100 μL of DMSO to each well. The absorbance was monitored at 570 nm (measurement) and 630 nm (reference) using a 96-well plate reader (Bio-Rad, Hercules, CA). Data were collected for three replicates each and used to calculate the mean. The percentage inhibition was calculated, from this data, using the formula

$$= \frac{\text{mean OD of untreated cells (control)} - \text{mean OD of treated cells}}{\text{mean OD of untreated cells (control)}}$$

$$\times 100$$

The IC$_{50}$ values were calculated using *Table Curve 2D*, version 5.01.

Hoechst 33258 Staining. The cell pathology was detected by staining the nuclear chromatin of trypsinized cells (4.0×10^4/mL) with 1 μL of Hoechst 33258 (1 mg/mL) for 10 min at 37 °C. Staining of suspension cells with Hoechst 33258 was used to detect apoptosis.[84] A drop of cell suspension was placed on a glass slide, and a coverslip was overlaid to reduce light diffraction. At random, 300 cells were observed in a fluorescent microscope (Carl Zeiss, Jena, Germany) fitted with a 377−355 nm filter and observed at 400× magnification, and the percentage of cells reflecting pathological changes was calculated. Data were collected for four replicates and used to calculate the mean and standard deviation.

AO/EB Staining. For both suspension and adherent cells, 96-well plates were centrifuged at 1000 rpm (129 g) for 5 min using a Beckman model TJ-6 centrifuge with inserts for 96-well plates. An EB/AO dye mix (8 μL) was added to each well, and cells were viewed under the same

microscope as that used above. Tests were done in triplicate, counting a minimum of 100 total cells each.

Comet Assay. DNA damage was quantified by means of the comet assay as described.[85,86] Assays were performed under red light at 4 °C. Cells used for the comet assay were sampled from a monolayer during the growing phase, 24 h after seeding. Cells were treated with copper(II) complexes at IC$_{50}$ dose, and cells were harvested by a trypsinization process at 12 and 24 h. A total of 200 μL of 1% normal agarose in PBS at 65 °C was dropped gently onto a fully frosted microslide, covered immediately with a coverslip, and placed over a frozen ice pack for about 5 min. The coverslip was removed after the gel had set. The cell suspension from one fraction was mixed with 1% low-melting agarose at 37 °C in a 1:3 ratio. A total of 100 μL of this mixture was applied quickly on top of the gel, coated over the microslide, and allowed to set as before. A third coating of 100 μL of 1% low-melting agarose was placed on the gel containing the cell suspension and allowed to set. Similarly, slides were prepared (in duplicate) for each cell fraction. After solidification of the agarose, the coverslips were removed, and the slides were immersed in an ice-cold lysis solution (2.5 M NaCl, 100 mM Na$_2$EDTA, 10 mM Tris, NaOH; pH 10, 0.1% Triton X-100) and placed in a refrigerator at 4 °C for 16 h. All of the above operations were performed in low-lighting conditions in order to avoid additional DNA damage. Slides, after removal from the lysis solution, were placed horizontally in an electrophoresis tank. The reservoirs were filled with an electrophoresis buffer (300 mM NaOH and 1 mM Na$_2$EDTA, pH > 13) until the slides were just immersed in it. The slides were allowed to stand in the buffer for about 20 min (to allow DNA unwinding), after which electrophoresis was carried out at 0.8 v/cm for 15 min. After electrophoresis, the slides were removed, washed thrice in a neutralization buffer (0.4 M Tris, pH 7.5), and gently dabbed to dry. Nuclear DNA was stained with 20 μL of EthBr (50 μg/mL). Photographs were taken using an epifluorescence microscope (Carl Zeiss). A total of 200 cells from each treatment were digitalized and analyzed with image analysis (CASP Software). The images were used to estimate the DNA content of individual nuclei and to evaluate the degree of DNA damage representing a fraction of the total DNA in the tail.

Mitochondrial Transmembrane Potential. The mitochondrial transmembrane potential was measured using the fluorescent probe JC-1, which produces green fluorescence in the cytoplasm and red-orange fluorescence when concentrated in respiring mitochondria having a negative internal potential. Cells treated overnight with complex **3** in 12-well plates were incubated for 30 min with 2 μg/mL of JC-1 in the culture medium. The adherent cell layer was then washed three times with PBS and dislodged with 250 μL of trypsin−EDTA. Cells were collected in PBS/2% bovine serum albumin (BSA), washed twice by centrifugation, resuspended in 0.3 mL of PBS/2% BSA, mixed gently, and examined in the fluorescent microscope using a UV filter (450−490 nm). A total of 300 cells per sample were counted in duplicate for each dose point. The specific fluorescent patterns were indicative of live and dead cells.

Western Blot Analysis. Total proteins from untreated and treated cells for 12 and 24 h were determined by a modified Lowery method using specific apoptotic markers such as p53, Bcl-2, Bax, and β-actin (loading control) antibodies (Sigma, Madison, WI). In T$_{75}$ plates, 5×10^6 cells were seeded and treated with the complexes at IC$_{50}$ concentration of **3**. After the indicated periods, cells were washed in cold PBS and lysed in 1% Triton X-100, 50 mmol/L Tris, pH 7.6, and 150 mmol/L NaCl containing 2 mmol of L-phenylmethylsulfonyl fluoride. Subsequently, proteins were separated by sodium dodecyl sulfate/polyacrylamide gel electrophoresis and transferred to a nitrocellulose membrane. The loading and transfer of equal amounts of protein was confirmed by staining the membrane with Ponceau S. Membranes were blocked with 5% nonfat dry milk powder in a Tris-buffered saline (TBS; 10 mmol/L Tris-HCl, pH 7.4, 100 mmol/L NaCl)

for 1 h and then incubated with the primary antibody at appropriate dilutions overnight at 4 °C. Membranes were washed four times with TBS/0.05% Tween-20 and incubated with secondary antibodies conjugated with peroxidase (Bangalore Genei, Bangalore, India) or alkaline phosphatase for 1 h. After extensive washing, the reaction was developed with diaminobenzidine/1—4CN substrate.

■ ASSOCIATED CONTENT

Ⓢ Supporting Information. X-ray crystallographic data in CIF format, electronic absorption spectral behavior, molar conductivity, time-dependent DNA cleavage data, concentration-dependent oxidative cleavage data, ESI-MS spectra, plot of A/A_0 vs R, saturation kinetics, time course of pUC19 cleavage, and Western blotting analyses. This material is available free of charge via the Internet at http://pubs.acs.org.

■ AUTHOR INFORMATION

Corresponding Author

*E-mail: palanim51@yahoo.com or palaniandavarm@gmail.com.

■ ACKNOWLEDGMENT

■ REFERENCES

(1) Rosenberg, B. *Naturwissenschaften* **1973**, *60*, 399.

(2) Lippert, B. *Cisplatin: Chemistry and Biochemistry of a Leading Anticancer Drug*; Lippert, B., Ed.; Wiley-VCH Verlag GmbH: Weinheim, Germany, 1999.

(3) (a) Cohen, S. M.; Lippard, S. J. *Prog. Nucleic Acid Res. Mol. Biol.* **2001**, *67*, 93. (b) Lloyd, D. *Trends Pharmacol. Sci.* **2002**, *23*, 158.

(4) Qu, Y.; Farrell, N. *J. Am. Chem. Soc.* **1991**, *113*, 4851.

(5) Kraker, A. J.; Hoeschele, J. D.; Elliott, W. L.; Showalter, H. D. H.; Sercel, D.; Farrell, N. P. *J. Med. Chem.* **1992**, *35*, 4526.

(6) Farrell, N.; Qu, Y.; Bierbach, U.; Valsecchi, M.; Menta, E. In *30 years of Cisplatin, Chemistry and Biochemistry of a leading Anticancer Drug*; Lippert, B., Ed.; Verlag CH: Basel, Switzerland, 1999; p 479.

(7) Sessa, C.; Capri, G.; Gianni, L.; Peccatori, F.; Grasselli, G.; Bauer, J.; Zucchetti, M.; Vigano, L.; Gatti, A.; Minoia, C.; Liati, P.; Vanden Bosch, S.; Bernareggi, A.; Camboni, G.; Marsoni, S. *Ann. Oncol.* **2000**, *11*, 977–983.

(8) Jodrell, D. I.; Evans, T. R. J.; Steward, W.; Cameron, D.; Prendiville, J.; Aschele, C.; Noberasco, C.; Lind, M.; Carmichael, J.; Dobbs, N.; Camboni, G.; Gatti, B.; De Braud, F. *Eur. J. Cancer* **2004**, *40*, 1872–1877.

(9) Hensing, T. A.; Hanna, N. H.; Gillenwater, H. H.; Camboni, M. G.; Allievi, C.; Socinski, M. A. *Anti-Cancer Drugs* **2006**, *17*, 697–704.

(10) Farrell, N. *Met. Ions Biol. Syst.* **2004**, *42*, 251–296.

(11) Brabec, V.; Kasparkova, J.; Vrana, O.; Novakova, O.; Cox, J. W.; Qu, Y.; Farrell, N. *Biochemistry* **1999**, *38*, 6781.

(12) Rosenberg, B.; Van Camp, L.; Trosko, J. E.; Mansour, V. H. *Nature* **1969**, *222*, 385.

(13) Jamieson, E. R.; Lippard, S. J. *Chem. Rev.* **1999**, *99*, 2467.

(14) (a) Cocchietto, M.; Sava, G. *Pharmacol. Toxicol.* **2000**, *87*, 193. (b) Zorzet, S.; Sorc, A.; Casarsa, C.; Cocchietto, M.; Sava, G. *Met.-Based Drugs* **2001**, *8*, 1. (c) Gagliardi, R.; Sava, G.; Pacor, S.; Mestroni, G.; Alessio, E. *Clin. Exp. Metastasis* **1994**, *12*, 93. (d) Magnarin, M.; Bergamo, A.; Carotenuto, M. E.; Zorzet, S.; Sava, V. *Anticancer Res.* **2000**, *20*, 2939. (e) Rademaker-Lakhai, J. M.; Van den Bongard, D.; Pluim, D.; Beijnen, J. H.; Schellens, J. H. *Clin. Cancer Res.* **2004**, *10*, 3717.

(15) May, P. M.; Williams, D. R. In *Metal Ions in Biological Systems*; Sigel, H., Ed.; Marcel Dekker: New York, 1981; Vol. 12, Chapter 7.

(16) Sigel, H., Ed. *Metal Ions in Biological Systems*; Marcel Dekker: New York, 1981; Vol. 13.

(17) Miura, T.; Hori-i, A.; Mototani, H.; Takeuchi, H. *Biochemistry* **1999**, *38*, 11560.

(18) Fernandes, C.; Parrilha, G. L.; Lessa, J. A.; Santiago, L. J. M.; Kanashiro, M. M.; Boniolo, F. S.; Bortoluzzi, A. J.; Vugman, N. V.; Herbst, M. H.; Horn, A., Jr. *Inorg. Chim. Acta* **2006**, *359*, 3167.

(19) Bales, B. C.; Kodama, T.; Weledji, Y. N.; Pitie, M.; Meunier, B.; Greenberg, M. M. *Nucleic Acid Res.* **2005**, *33*, 5371.

(20) Uma Maheswari, P.; Roy, S.; Dulk, H. D.; Barends, S.; Wezel, G. V.; Kozlevcar, B.; Gamez, P.; Reedijk, J. *J. Am. Chem. Soc.* **2006**, *128*, 710.

(21) Ranford, J. D.; Sadler, P. J.; Tocher, D. A. *Dalton Trans.* **1993**, 3393.

(22) Ng, C. H.; Kong, K. C.; Von, S. T.; Balraj, P.; Jensen, P.; Thirthagiri, E.; Hamada, H.; Chikira, M. *Dalton Trans.* **2008**, 447.

(23) Zhang, S.; Zhu, Y.; Tu, C.; Wei, H.; Yang, Z.; Lin, L.; Ding, J.; Zhang, J.; Guo, Z. *J. Inorg. Biochem.* **2004**, *98*, 2099.

(24) Rajendiran, V.; Karthik, R.; Palaniandavar, M.; Evans, H. S.; Periasamay, V. S.; Akbarsha, M. A.; Srinag, B. S.; Krishnamurthy, H. *Inorg. Chem.* **2007**, *46*, 8208.

(25) Ramakrishnan, S.; Rajendiran, V.; Palaniandavar, M.; Periasamay, V. S.; Akbarsha, M. A.; Srinag, B. S.; Krishnamurthy, H. *Inorg. Chem.* **2009**, *48*, 1309.

(26) Humphreys, K. J.; Karlin, K. D.; Rokita, S. E. *J. Am. Chem. Soc.* **2002**, *124*, 6009.

(27) Li, L.; Karlin, K. D.; Rokita, S. E. *J. Am. Chem. Soc.* **2005**, *127*, 520.

(28) Gonzalez-Alvarez, M.; Alzuet, G.; Borras, J.; Macias, B.; Castineiras, A. *Inorg. Chem.* **2003**, *42*, 2992.

(29) (a) Humphreys, K. J.; Karlin, K. D.; Rokita, S. E. *J. Am. Chem. Soc.* **2001**, *123*, 5588. (b) Humphreys, K. J.; Karlin, K. D.; Rokita, S. E. *J. Am. Chem. Soc.* **2002**, *124*, 8055. (c) Humphreys, K. J.; Johnson, A. E.; Karlin, K. D.; Rokita, S. E. *J. Biol. Inorg. Chem.* **2002**, *7*, 835.

(30) (a) Komiyama, M.; Kina, S.; Matsumura, K.; Sumaoka, J.; Tobey, S.; Lynch, V. M.; Anslyn, E. *J. Am. Chem. Soc.* **2002**, *124*, 13731. (b) Kirin, S. I.; Happel, C. M.; Hrubanova, S.; Weyhermüller, T.; Klein, C.; Metzler-Nolte, N. *Dalton Trans.* **2004**, 1201.

(31) Humpreys, K. J.; Hohnson, A. J.; Karlin, K. D.; Rokita, S. E. *J. Biol. Inorg. Chem.* **2002**, *7*, 835.

(32) Li, L.; Karlin, K. D.; Rokita, S. E. *J. Am. Chem. Soc.* **2005**, *127* (2), 520.

(33) (a) Rajendiran, V.; Murali, M.; Suresh, E.; Periasamay, V. S.; Akbarsha, M. A.; Palaniandavar, M. *Dalton Trans.* **2008**, 2157. (b) Rajendiran, V.; Murali, M.; Suresh, E.; Sinha, S.; Somasundaram, K.; Palaniandavar, M. *Dalton Trans.* **2008**, 148.

(34) Huheey, J. E.; Keiter, E. A.; Keiter, R. L.; Medhu, O. K. *Inorganic Chemistry, Principles of Structure and Reactivity*; Pearson Education: Upper Saddle River, NJ, 2006, pp 425—426.

(35) Collins, J. G.; Sleeman, A. D.; Aldrich-Wright, J. R.; Greguric, I.; Hambly, T. W. *Inorg. Chem.* **1998**, *37*, 3133.

(36) Ramakrishnan, S.; Palaniandavar, M. *Dalton Trans.* **2008**, 3866.

(37) Winpenny, R. *Adv. Inorg. Chem.* **2001**, *52*, 1.

(38) Tysoe, S. A.; Morgan, R. J.; Baker, A. D.; Strekas, T. C. *J. Phys. Chem.* **1993**, *97*, 1707.

(39) Kelly, J. M.; Tossi, A. B.; McConnell, D. J.; Strekas, T. C. *Nucleic Acids Res.* **1985**, *13*, 1707.

(40) Haworth, I. S.; Elcock, A. H.; Freemann, J.; Rodger, A.; Richards, W. G. J. *J. Biomol. Struct. Dyn.* **1991**, *9*, 23.

6470

dx.doi.org/10.1021/ic1024185 |*Inorg. Chem.* 2011, 50, 6458–6471

(41) Carter, M. T.; Rodriguez, M.; Bard, A. J. *J. Am. Chem. Soc.* **1989**, *111*, 8901.

(42) Boger, D. L.; Fink, S. R.; Brunette, S. R.; Tse, W. C.; Hedrick, M. P. *J. Am. Chem. Soc.* **2001**, *123*, 5878.

(43) Friedman, A. E.; Chamron, J. C.; Sauvage, J. P.; Turro, N. J.; Barton, J. K. *J. Am. Chem. Soc.* **1990**, *112*, 4960.

(44) Uma Maheswari, P.; Rajendiran, V.; Evans, H. S.; Palaniandavar, M. *Inorg. Chem.* **2006**, *45*, 37.

(45) Uma Maheswari, P.; Palaniandavar, M. *J. Inorg. Biochem.* **2004**, *98*, 219.

(46) Selvakumar, B.; Rajendiran, V.; Uma Maheswari, P.; Evans, H. S.; Palaniandavar, M. *J. Inorg. Biochem.* **2006**, *100*, 316.

(47) Ramakrishnan, S.; Palaniandavar, M. *J. Chem. Sci.* **2005**, *117*, 179.

(48) Uma Maheswari, P.; Rajendiran, V.; Parthasarathi, R.; Subramanian, V.; Palaniandavar, M. *Bull. Chem. Soc. Jpn.* **2005**, *78*, 835.

(49) Baguley, B. C.; LeBret, M. *Biochemistry* **1984**, *23*, 937.

(50) Lee, M.; Rhodes, A. L.; Wyatt, M. D.; Forrow, S.; Hartley, J. A. *Biochemistry* **1993**, *32*, 4237.

(51) Gabbay, E. J.; Scofield, R. E.; Baxter, C. S. *J. Am. Chem. Soc.* **1973**, *95*, 7850.

(52) Ramakrishnan, S.; Suresh, E.; Riyasdeen, A.; Akbharsha, M. A.; Palanianadavar, M. *Dalton.Trans.* Under minor revision.

(53) Ramakrishnan, S.; Suresh, E.; Riyasdeen, A.; Akbharsha, M. A.; Palanianadavar, M. *Dalton.Trans.* Under minor revision.

(54) Dhar, S.; Reddy, P. A. N.; Chakravarty, A. R. *Dalton Trans.* **2004**, 697.

(55) Sreedhara, A.; Freed, J. D.; Cowan, J. A. *J. Am. Chem. Soc.* **2000**, *122*, 8814.

(56) Gonalez-Alvarez, M.; Alzuet, G.; Borras, J.; Pitie, M.; Meunier, B. *J. Biol. Inorg. Chem.* **2003**, *8*, 644.

(57) Garcia-Gimenez, J. L.; Alzuet, G.; Gonzalez-Alvarez, M.; Castineiras, A.; Liu-Gonzalez, M.; Borras, J. *Inorg. Chem.* **2007**, *46*, 7178.

(58) Chen, J.; Wang, X.; Shao, Y.; Zhu, J.; Zhu, Y.; Li, Y.; Xu, Q.; Guo, G. *Inorg. Chem.* **2007**, *46*, 3036.

(59) Mazumder, A.; Sutton, C. L.; Sigman, D. S. *Inorg. Chem.* **1993**, *32*, 3516–3560.

(60) Tu, C.; Shao, Y.; Gan, N.; Xu, Q.; Guo, Z. *Inorg. Chem.* **2004**, *43*, 4761.

(61) Thomas, A. M.; Nethaji, M.; Mahadevan, S.; Chakravarty, A. R. *J. Inorg. Biochem.* **2003**, *94*, 171.

(62) Santra, B. K.; Reddy, P. A. N.; Neelakanta, G.; Mahadevan, S.; Nethaji, M.; Chakravarty, A. R. *J. Inorg. Biochem.* **2002**, *89*, 191.

(63) Thyagarajan, S.; Murthy, N. N.; Narducci, A.; Sarjeant, A.; Karlin, K. D.; Rokita, S. E. *J. Am. Chem. Soc.* **2006**, *128*, 7003.

(64) Pyle, A. M.; Barton, J. K. *Prog. Inorg. Chem.* **1990**, *38*, 413.

(65) Perrin, D. M.; Mazumder, A.; Sigman, D. S. In *Progress in Nucleic Acid Chemistry and Molecular Biology*; Cohn, W., Moldave, K., Eds.; Academic Press: New York, 1996; Vol. 52, p 123.

(66) Sigman, S. *Acc. Chem. Res.* **1986**, *19*, 180.

(67) Magne, N.; Fischel, J. L.; Dubreuil, J. L.; Formento, A.; Marcie, S.; Lagrange, J. L.; Milano, G. *Br. J. Cancer* **2002**, *86*, 819.

(68) Komeda, S.; Lutz, M.; Spek, A. L.; Chikuma, M.; Reedijk, J. *Inorg. Chem.* **2000**, *39*, 4230.

(69) Komeda, S.; Lutz, M.; Spek, A. L.; Yamanaka, Y.; Sato, T.; Chikuma, M.; Reedijk, J. *J. Am. Chem. Soc.* **2002**, *124*, 4738.

(70) Ghobrial, I. M.; Witzig, T. E.; Adjei, A. A. *Cancer J. Clin.* **2005**, *55*, 178.

(71) Alapetite, C.; Wachter, T.; Sage, E.; Moustacchi, E. *Int. J. Radiat. Biol.* **1996**, *69*, 359.

(72) Phil Dash Basic Medical Sciences, St.George's, University of London, www.sgul.ac.uk/dept/immunology/~dash.

(73) Vousden, K. H.; Lu, X. *Nat. Rev. Cancer* **2002**, *2*, 594.

(74) Coutts, A. S.; La Thangue, N. *Biochem. Soc. Symp.* **2006**, 181.

(75) Xu, J.; Lian, L.-J.; Wu, C.; Wang, X.-F.; Fu, W.-Y.; Xu, L.-H. *Food Chem. Toxicol.* **2008**, *46*, 1488.

(76) Vogel, A. I.; Tatchell, A. R.; Furnis, B. S.; Hannaford, A. J.; Smith, P. W. G. *Vogel's Textbook of Practical Organic Chemistry*, 5th ed.; Prentice Hall: New York, 1989.

(77) Murmur, J. *J. Mol. Biol.* **1961**, *3*, 208.

(78) *SMART & SAINT Software Reference Manuals*, version 5.0; Bruker AXS Inc.: Madison, WI, 1998.

(79) Sheldrick, G. M. *SAINT*, version 5.1; Siemens Industrial Automation Inc.: Madison, WI, 1995.

(80) *SADABS, Empirical Absorption Correction Program*; University of Göttingen: Göttingen, Germany, 1997.

(81) (a) Sheldrick, G. M. *SHELXTL Reference Manual*, version 5.1; Bruker AXS: Madison, WI, 1997. (b) Sheldrick, G. M. *SHELXS-97: Program for the Solution of Crystal Structure*; University of Göttingen: Göttingen, Germany, 1997. (c) Sheldrick, G. M. *Acta Crystallogr.* **2008**, *A64*, 112–122.

(82) Singh, N. P.; McCoy, M. T.; Tice, R. R.; Schneider, E. L. *Exp. Cell Res.* **1988**, *175*, 184.

(83) Blagosklonny, M.; El-Diery, W. S. *Int. J. Cancer* **1996**, *67*, 386.

(84) Kasibhatla, G. P. A. H.; Finucane, D.; Brunner, T.; Wetzel, E. B.; Green, D. R. *Protocol: Staining of suspension cells with Hoechst 33258 to detect apoptosis. Cell: A laboratory manual Culture and Biochemical Analysis of Cells*; CSHL Press: Cold Spring Harbor, NY, 2000; Vol. 1, p 15.5.

(85) Sihn, C. R.; Suh, E. J.; Lee, K. H.; Kim, T. Y.; Kim, S. H. *Cancer Lett.* **2003**, *201*, 203.

(86) Heffeter, P.; Jakupec, M. A.; Körner, W.; Wild, S.; Von Keyserlingk, N. G.; Elbling, L.; Zorbas, H.; Koryneuska, A.; Knasmüller, S.; Sutterlüty, H.; Micksche, M.; Keppler, B. K.; Berger, W. *Biochem. Pharmacol.* **2006**, *71*, 426.

6471

dx.doi.org/10.1021/ic1024185 |*Inorg. Chem.* 2011, 50, 6458–6471